Evaluating the Impact of Conjugation Break Spacer Incorporation in Poly(3,4-

Propylenedioxythiophene)-based Cathode Binders for Lithium-Ion Batteries

Pratyusha Das,^{1#} Charlene Z. Salamat,^{2#} Billal Zayat,¹ Rodrigo Elizalde-Segovia,¹ Yunfei Wang,³ Xiaodan Gu,³ Sri R. Narayan,^{1^} Sarah H. Tolbert^{2,4*} and Barry C. Thompson^{1*}

¹Department of Chemistry and Loker Hydrocarbon Research Institute, University of Southern California, Los Angeles, California 90089-1661, USA

²Department of Chemistry and Biochemistry, UCLA, Los Angeles, California 90095-1569, USA

³School of Polymer Science and Engineering, The University of Southern Mississippi, Hattiesburg, Mississippi 39406, United States

⁴Department of Materials Science and Engineering, UCLA, Los Angeles, California 90095, USA

KEYWORDS: conductive polymer binder, conjugation break spacer, stretchability, lithiumion battery, conductivity, rate capability.

ABSTRACT: Conductive polymer binders have gained significant attion in the last decade as functional binders providing electronic and ionic conductivity alongside mechanical adhesion of composite electrodes in lithium-ion batteries (LIBs). The driving force behind such advancements stems from the poor binding strength, limited mechanical properties and absence of electronic conductivity of the commonly used non-conjugated polymer binder, poly(vinylidene fluoride) (PVDF). With a goal to induce stretchability and deformability to the otherwise brittle conjugated backbone, we report here dihexyl-substituted poly(3,4propylenedioxythiophene)-based (PProDOT-Hx2) conjugated polymers wherein conjugation break spacers (CBS, T-X-T) of varying alkyl spacer length (X = 6, 8, 10) and varying content (5%, 10% and 20%) have been randomly incorporated into the PProDOT backbone generating a family of nine random PProDOT-CBS copolymers. Electrochemical characterization revealed that three out of the nine PProDOT-CBS polymers (5% T-6-T, 5% T-8-T and 10% T-6-T) are electrochemically stable over long-term cycling of 100 cycles. Electronic conductivity of the PProDOT-CBS polymers is consistent with previous literature reports on CBS polymers where decline in charge carrier mobility is observed with increase in CBS content and spacer length, although no significant difference in ionic conductivity in these polymers was observed. This is supported by GIWAXS studies indicating a decrease in lamellar peak intensity

with increasing CBS content and spacer length. Mechanical properties of the three selected PProDOT-CBS polymers were investigated using the established "film-on-water" technique and a novel technique that we report here for the first time, "film-on-solvent," where the solvent used is the same as employed in the battery electrolyte. Both techniques showcase a generally lower tensile modulus (E) and higher crack onset strain (COS) of the PProDOT-CBS polymers relative to fully conjugated PProDOT-Hx2. Furthermore, significant enhancement in mechanical properties is observed with the "film-on-solvent" method suggesting that solvent-induced swelling in the battery electrolyte plays an important role in the stretchability and deformability of the polymer binders. Finally, cell testing of the PProDOT-CBS polymers with NCA cathodes aligned well with the electrochemical and mechanical studies, where 10% T-6-T displayed the highest retention in capacity after 300 cycles, attributed to its highest crack onset strain. Rate capability measurements proved that higher electronic conductivity is favored over mechanical properties during high rates of discharge as observed in the case of 5% T-8-T exhibiting the highest capacity retention at a high discharge rate of 8C. This work illustrates that strategic introduction of CBS units into conjugated polymer binders is a viable method for generation of stretchable conductive polymer binders for emerging high-capacity electrodes in LIBs.

INTRODUCTION:

Lithium-ion batteries (LIBs) have gained tremendous attention in the world market over the last few decades to meet global energy demands for consumer electronics, portable electronic

devices, and electric vehicles (EVs), owing to their high-energy and power density, high efficiency, long cycle life, light weight and portability compared to first-generation batteries.¹ Development of high-capacity materials for high-theoretical capacity of electrochemical lithiation has been on the rise to enhance the energy density of the current electrode materials and are at present reaching their theoretical limits.² However, both high-voltage cathodes such as LiMn₂O₄ and high-capacity anodes like Silicon (Si) undergo huge volumetric expansion and contraction under repeated lithiation/delithiation (cycling), leading to electrode fracture.^{3,4} Typically, nanoscale carbon additives and a polymer binder (usually polyvinylidene fluoride, PVDF) are integrated into the composite electrode structure to maintain a network that electrically and mechanically connects the individual active material particles. Rupture of such composite electrodes on cycling causes the active material particles to detach from the polymer binder-carbon network, thus leading to capacity fade on subsequent cycles. Hence, establishing an intimate contact between the individual components of the composite electrode is key to maintaining electrochemical activity and contribution to overall capacity.

Numerous strategies have been developed to mitigate the mechanical degradation of LIB electrodes, arising from their continuous expansion and contraction during the repeated lithiation/delithiation process. These include design of composite electrode formulations,⁵⁻⁷ dimensional reduction of active materials,⁸⁻¹⁰ 3D architectures¹¹⁻¹³ and controlling the overall electrode morphology and microstructure.¹⁴⁻¹⁶ However, while such approaches have been successful in leveraging electronic and ionic charge transport and minimization of cracking

and pulverization of high-capacity electrodes, they are nevertheless limited by issues such as reduced content of active materials, low volumetric energy density, processing complexity and expensive synthetic routes. Recently polymer binders, typically an inactive component in LIBs, have gained importance in impacting the overall performance of LIBs. 17,18 Weak van der Waals binding forces and the electrically insulating nature of the commonly used PVDF, have resulted in limited adhesive strength, and poor flexibility and elasticity, thereby failing to suffice as a promising polymer binder for emerging high-capacity and high-energy density electrodes which undergo huge volume expansion and contraction during charge/discharge cycles. 19,20 In this regard, natural, water-soluble binders such as carboxymethyl chitosan (CMC), alginate (Alg), guar gum (GG), gum Arabic (GA) and synthetic binders such as poly(acrylic acid) (PAA), polyamide imide (PAI), poly(vinyl alcohol) (PVA) have been widely investigated, owing to their higher tensile strength and superior mechanical properties in comparison to PVDF.^{21,22} Such polymers containing carboxylate, hydroxyl, acetyl, imide or ester type polar functional groups bestow flexibility and elastomeric properties to highcapacity electrodes, leading to electrode structural stability and enhancement in long-term cycling.²³ However, these binders are limited by their poor electronic conductivity resulting in loss of electrical contact during volume expansion and contraction of electrodes. Hence, conductive polymer binders with π -conjugated backbones have gained significant attention in the last decade, leveraging electronic conductivity alongside mechanical adhesion.^{24,25}

Simultaneous conduction of electrons and Li⁺ ions is an important criteria for maintaining charge transport pathways in a battery environment, which ultimately impacts its rate capability and cycle life. 26,27 Such mixed conduction in polymer binders is typically achieved via multicomponent heterogenous blends of electron and ion conducting polymers, ^{28–30} block copolymers^{31–33} and single-component mixed electron and Li⁺ ion conducting polymers.^{26,34} In order to alleviate the structural degradation of high-capacity composite electrodes without loss of electronic conduction, stretchable and ductile conductive polymer binders are desired. A notable amount of research has been done in this area in the recent past, especially for Si anodes in LIBs. 29,35-37 Most of the reported literature that addresses mechanical properties of conductive polymer binders in LIBs include multicomponent composite binders, 28,37 3D nanostructured conductive polymer gels, 38,39 crosslinked networks and self-healing polymers for attaining a robust electrode architecture. 40-42 For example, Wang et al. reported a stretchable conductive glue (CG) polymer for Si anodes, exhibiting stretchability up to 400% without any loss of conductivity and mechanical integrity, thereby withstanding the large volume change of Si nanoparticles during continuous cycling.²⁹ The CG possessing high mechanical ductility and high conductivity at large strains is obtained by cross-linking Dsorbitol and vinyl acetate-acrylic (VAA) onto the electrically conducting polymer poly(3,4ethylenedioxythiophene):polystyrene sulfonate (PEDOT:PSS). The CG facilitated the stable growth of solid electrolyte interphase (SEI), resulting in high coulombic efficiency. This work led to a high achievable areal capacity of 5.13 mA h cm⁻² at a high mass loading of 2 mg cm⁻² for Si-CG composite anode. Recently, Kim et al. also used PEDOT:PSS for generating a

hierarchically structured conductive polymer binder along with silver (Ag) nanowires for Si anodes in LIBs.³⁷ In their work, composites of PEDOT:PSS and poly(vinyl alcohol) (PVA) were mixed with poly(ethylene glycol) (PEG) and poly(ethylene oxide) (PEO) to generate hierarchical structures on account of different chain lengths of PEG and PEO. Through H-bonding and crosslinking, the resulting binder (5-P) when used with Si anodes demonstrated higher electrical conductivity (40 %) and stretchability (60 %) in comparison to PEG or PEO, resulting in high battery performance. Furthermore, addition of AgNW to the binder led to superior adhesion with the current collector, faster electron transport and buffer space for volume expansion. Hence, the highest specific capacity for Si anodes was achieved after 100 cycles when the binder was used with AgNW (Si/5-P/AgNW) compared to Si/5-P and Si-CMC electrodes.

While the above reports on stretchable conductive polymer binders showcase the maintenance of high conductivity at large strains for high-capacity electrodes like Si anodes, these binders are mostly multi-component systems, which reduces the overall percentage of active material loading. Additionally, most of the mechanical investigations on conductive polymer binders have been demonstrated on films derived from colloidal aqueous suspensions such as PEDOT:PSS.⁴³ Although aqueous processing of such heterogenous blends is sustainable, their film-forming ability is poor compared to homogenous systems.⁴⁴ This calls for a more general chemical design strategy for intrinsically stretchable conductive polymer binders for electrodes in LIBs, which are single-component homogenous systems that can be applied

across all cathodes and anodes in LIBs. Despite the inherent competition between mechanical deformability and electronic charge transport^{45–48} in conjugated polymers, a number of strategies have been adopted as promising pathways for co-optimization of intrinsic deformability and electronic performance. These include polymer blending of rigid conjugated polymers with soft, deformable elastomers^{49–51} and intrinsically stretchable conjugated polymers such as block copolymers with hard and soft building blocks;⁵² employing conjugation break spacers (CBS) in random copolymers;^{53,54} adopting long, flexible side chains on the conjugated backbone;^{55,56} and utilization of self-healing and crosslinking moieties, among others.^{57–59} Additionally, morphological control and thin-film microstructure also play a key role in evaluation of charge transport and mechanical deformability, where percolation morphology, solution aggregation, tie chain effects and film formation dynamics play a big role in overall electrical and mechanical properties of conjugated polymer films.⁴⁵

Incorporation of conjugation break spacers in π -conjugated backbones has recently been a popular approach to induce stretchability in conjugated polymers for diverse applications. Conjugation break spacers are electrically insulating and generally aliphatic spacers incorporated between π -conjugated segments, providing unique control over mechanical properties and material processing without impeding semiconducting ability. CBS units act as "flexible linkers" disrupting the continuous conjugation of π -conjugated polymers adding conformational freedom or randomness to the otherwise rigid backbone. This "flexible linker" approach has provided insight into the nature of inter and intramolecular charge transport in

semiconducting polymers.⁶⁶ However, to date, no conductive polymer binders with CBS units have been reported with a goal of inducing stretchability to the overall binder system in LIBs.

Recently, we reported the use of the known polymer dihexyl-substituted poly(3,4-propylenedioxythiophene) (PProDOT-Hx2) as an electrochemically stable, dual electron and Li¹ ion conducting polymer binder exhibiting excellent performance for LiNiosCoo15Aloo5O2 (NCA) cathodes. 34.67 To maximize mixed conduction, the ionic conductivity of PProDOT-Hx2 was further enhanced by replacing hexyl (Hex) side chains to varying extents with oligoether (OE) side chains, generating a family of synthetically tunable, electrochemically stable, random copolymers (Hex:OE) PProDOTs, allowing fine-tuning of electronic and ionic conductivity. 26 Having established PProDOTs as effective dual electron and Li¹ ion conductive cathode binder for LIBs, the next step for advanced polymer binder design is to induce flexibility and stretchability for application in emerging high-capacity electrodes. Hence, we directed our efforts to incorporate conjugation break spacers as flexible linkers in our previously reported PProDOT-Hx2 backbone and evaluated the impact on electrochemical, morphological and mechanical properties of the resulting binders.

Hex Hex Hex
$$K_2CO_3$$
, NDA K_2CO_3

X = 6, 8, 10

(m:n) = (0.95:0.05) (5% T-X-T)

(0.90:0.10) (10% T-X-T)

(0.80 : 0.20) (20% T-X-T)

Figure 1. Synthesis of PProDOT-CBS Random Copolymers using Direct Arylation Polymerization (DArP).

Here we explore a family of nine random copolymers based on PProDOT-Hx2, where bisthiophene-CBS units (T-X-T) of varying spacer lengths (X = 6, 8, 10 methylene -(CH2)- units) have been incorporated to varying extents (5%, 10%, 20%), via a random copolymerization strategy, generating a series of random copolymers (**PProDOT-CBS**) (**Fig. 1**). The individual PProDOT-CBS polymers are named by the spacer length of the CBS unit and their percentage incorporation. For example, the 5% T-8-T polymer has a T-8-T spacer incorporated randomly in the PProDOT-Hx2 backbone and comprises only 5% of the total monomer composition. A thorough experimental study of the resulting family of nine random copolymers has been demonstrated in this work to investigate the role of CBS incorporation on the electrochemical, mechanical and morphological properties of the polymers and for their ultimate application as conductive cathode binders for NCA cathodes compared to our previously reported PProDOT-

Hx₂ binder. Through electrochemical investigation, conductivity studies and morphological characterization, three out of the nine polymers (5% T-6-T, 5% T-8-T, and 10% T-6-T) were found suitable for cathode binder applications and were further explored for mechanical properties and battery performance. We observe that inclusion of CBS units indeed makes the PProDOT-Hx₂ backbone more ductile, which is evident in the long-term cycling performance and mechanical measurements. While the electronic conductivity decreases with increasing CBS length and percentage incorporation, judicious introduction of the CBS polymers leads to co-optimization of electronic conductivity and mechanical deformability, as clearly observed in the rate capability performance with NCA electrodes.

RESULTS AND DISCUSSIONS:

Synthesis of PProDOT-CBS Random Copolymers Using DArP:

PProDOT-CBS random copolymers were synthesized using the sustainable method of direct arylation polymerization (DArP) by modifying our previously reported condition (**Fig. 1**).²⁶ We have incorporated CBS units (T-X-T) of varying spacer length (X = 6, 8, 10) and varying content (5%, 10% and 20%) into our previously reported PProDOT-Hx₂ backbone³⁴ via a random copolymerization strategy. Tuning the spacer length and content resulted in a family of nine PProDOT-CBS polymers (**Table S1**). This is also the first report of introduction of CBS

units into a conjugated polymer backbone via DArP. All nine polymers were found to be insoluble in the battery electrolyte (EC/DMC 1:1) and were synthesized in good yield and molecular weight (13.2 – 37.2 kDa) (**Table S1**). Proton nuclear magnetic resonance spectroscopy (¹H NMR) (**Fig. S4-S15**) supports a close match between monomer feed ratio and polymer composition. All ¹H NMR spectra, gel permeation chromatography (GPC) traces of all the polymers (**Fig. S16-S24**) and details regarding the synthesis of monomers and polymers (**Scheme S1-S3**) can be found in the Supporting Information.

Electrochemical Properties of PProDOT-CBS Random Copolymers

To examine the effectiveness of the synthesized random copolymers as potential binders in LIB cathodes, their electrochemical thin-film behavior was first examined in a three-electrode cell with 1 M bis-(trifluoromethane)sulfonimide lithium salt (LiTFSI) in ethylene carbonate/dimethyl carbonate (EC/DMC) as the electrolyte and Li foil as the reference and counter electrodes. All measurements were performed inside an argon glovebox and initial CV curves were collected at a scan rate of 50 mV s⁻¹ between 2.8 and 4.1 V vs Li/Li⁺. The initial CV curves of the T-6-T copolymer family are shown in **Fig. 2**.

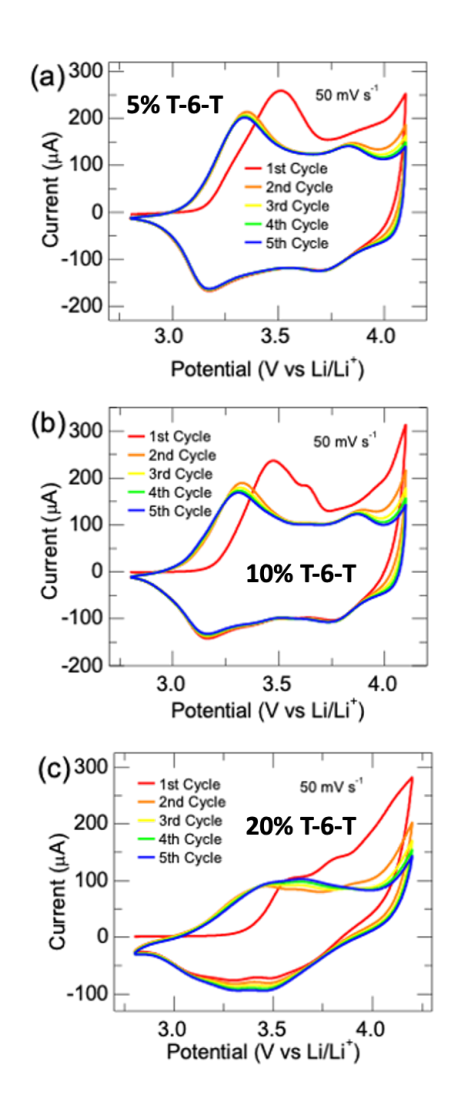


Figure 2. Initial CV data for (a) 5%, (b) 10%, and (c) 20% T-6-T in the potential range of 3-4.2 V at a scan rate of 50 mV s⁻¹ for cycles 1-5.

In the first cycle, and oxidation peak appears at 3.51 V vs Li/Li⁺ for 5% T-6-T, 3.47 V for 10% T-6-T, and 3.59 V for 20% T-6-T (**Fig. 2a-c**). In subsequent cycles, the oxidation peak shifts to 3.35 V, 3.31 V, and 3.46 V for 5%, 10%, and 20% T-6-T, respectively. A second oxidation peak also appears at 3.85 V and 3.87 V for 5% and 10% T-6-T. For all cycles, there is a first reduction peak at 3.17 V and an additional reduction peak at 3.70 and 3.74 V for 5% and 10% T-6-T,

respectively. Interestingly, only a very broad oxidation peak is seen for 20% T-6-T along with 2 broad overlapping reduction peaks at 3.31 and 3.48 V vs Li/Li⁺ (Fig. 2c). Similar redox peak shapes were observed for the T-8-T copolymer family (Fig. S25a-c), but with somewhat broader peaks. For the T-10-T family, the first cycle shows several oxidation peaks starting at 3.45 V. With subsequent cycles, however, the expected two oxidation peaks appear at 3.33 V and 3.84 V, and two reduction peaks are seen at 3.15 V and 3.84 V vs Li/Li⁺, respectively, for the 5% and 10% T-10-T polymers (Fig. S26a-c). For 20% T-10-T, a significant loss in capacity in subsequent cycles were observed suggesting that doping is not electrochemically reversible (**Fig. S26c**). Overall, this data suggests that the electrochemical doping process is highly reversible for all of the 5% and 10% T-X-T polymers. With the 20% copolymers, it appears that the non-conjugated segments may be limiting the electrochemical reversibility. It is interesting to note that the second redox peak around 3.8 V vs. Li/Li⁺ is not present in the first cycle for any of these polymers. In contrast, this peak is present in pure PProDOT-Hx2 from the start, suggesting structural rearrangement of the CBS polymers to a more standard structure upon electrochemical doping.

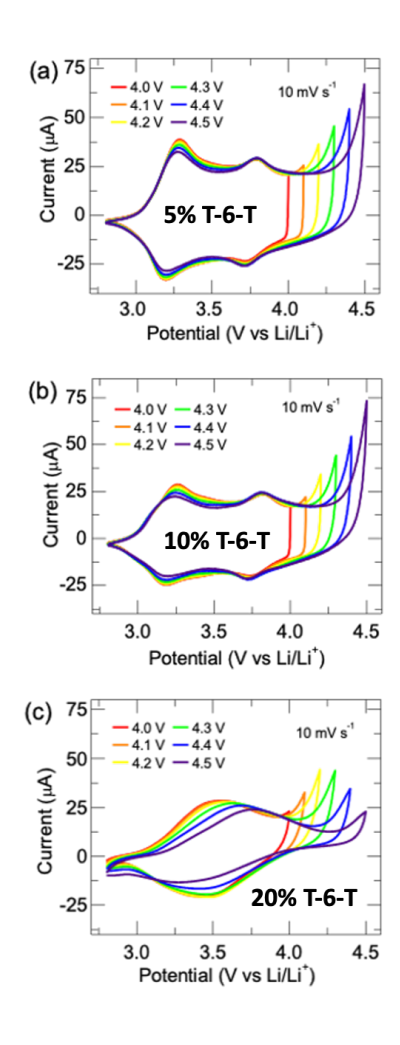


Figure 3. CV data for (a) 5%, (b) 10%, and (c) 20% T-6-T at various potential windows at 10 mV s $^{-1}$.

We expanded the potential window to higher potential to investigate the stable operational range of the PProDOT-CBS polymers. CV curves were obtained with gradually increasing potential ranges at 10 mV s⁻¹. **Fig. 3** shows the obtained CV curves for the T-6-T copolymer family. The shapes of the redox peaks were maintained for 5% T-6-T and 10% T-6-T when expanding the range beyond 4.2V up to 4.5V, however significant tailing was observed at higher voltages, especially when exceeding 4.3V. In contrast, large shifts in the redox peak

were observed for 20% T-6-T indicating its instability in the wide potential window (**Fig. 3c**). The shapes of the redox peaks for 5% T-8-T were retained up to a voltage cutoff of 4.5 V (**Fig. S27a**) and only small shifts in the redox peaks were observed when expanding the potential window for 10% T-8-T (**Fig. S7b**). CV data for 20% T-8-T showed significant shifts in the redox peaks suggesting electrochemical instability (**Fig. S7c**). For the T-10-T copolymer family, small shifts were observed even at 5% incorporation, as well as a reduction in peak current as the potential window was opened, suggesting that T-10-T family is less electrochemically stable (**Fig. S28a-b**).

To ensure that electrochemical doping and de-doping of the PProDOT-CBS polymer binders does not limit cathode cycling, we also examined the kinetics of electrochemical doping at high rates, by a series of CV measurements at various scan rates from 20-100 mV s⁻¹ (**Fig. 4**, **S29**, **S30**). To quantify the kinetics of polymer doping, we examined the relationship between the measured current and scan rate where a *b* value was calculated for each redox peak. A value of *b* equal to 0.5 indicates a process controlled by semi-infinite diffusion, while a *b* value close to 1 indicates a non-diffusion controlled or a surface-controlled charge-storage process. **Fig. 4a-c** shows that the *b* values for all redox peaks are above 0.9 for 5% and 10% T-6-T, but not for the 20% T-6-T. These *b* values indicate rapid redox processes in the 5% and 10% T-6-T films, but indicate that degradation is likely interfering with doping kinetics in the 20% T-6-T material. Similar results were obtained for T-8-T family and for 5% and 10% T-10-T copolymers (**Fig. S29a-c and S30a-b**). Such fast kinetics for the electrochemical *p*-doping of

the PProDOT-CBS polymers are expected to facilitate rapid electron transport when used as conductive cathode binders in LIBs.

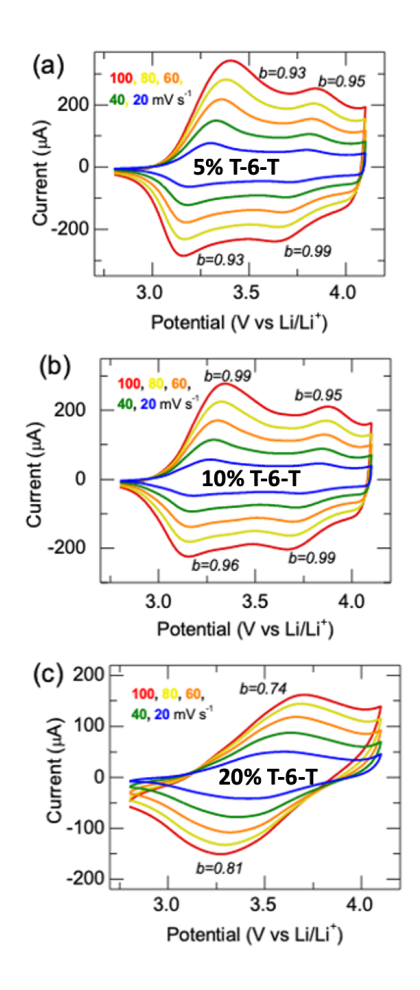


Figure 4. CV data for (a) 5%, (b) 10%, and (c) 20% T-6-T at various scan rates, ranging from 20 mV/s to 100 mV/s. The 5% and the 10% T-6-T show decent reversibility and rapid redox processes, while the 20% does not.

To examine the long-term electrochemical stability of the PProDOT-CBS polymers, they were continuously cycled between 2.8 V and 4.1 V vs Li/Li⁺ at a scan rate of 10 mV s⁻¹ for 100 cycles. **Fig. 5a and 5b** show that a significant fraction of the capacity is retained for 5% T-6-T and

10% T-6-T after 100 cycles (64 and 59%, respectively). In addition, no major peak shifts were observed indicating stable electrochemistry. However, we observe a significant drop in capacity for 20% T-6-T to just 21% after 100 cycles (Fig. S31). The CV data in Fig. 5c shows that 5% T-8-T retains a high capacity of 61% after 100 cycles. Although 10% T-8-T retains 54% of its initial capacity after 100 cycles (Fig. S32a), peak shifts were observed after 100 cycles making it electrochemically unstable for long-term cycling. Likewise, 20% T-8-T loses most of its capacity and is not suitable for long-term cycling (Fig. S32b). The CV data for T-10-T family (Fig. S33a-b) also shows similar behavior where 5% T-10-T has good capacity retention after 100 cycles with no significant change in redox peak shapes or positions. On the contrary, 10% T-10-T loses most of its initial capacity and is not suitable for long-term cycling. Thus, based on our overall electrochemical analysis, from the set of nine PProDOT-CBS polymers, 5% T-6-T, 5% T-8-T, and 10% T-6-T show stability and fast kinetics suitable for use as battery binders. All the other PProDOT-CBS polymers contain either too much or too long of conjugation breaks to support electrochemical parameters suitable for battery applications.

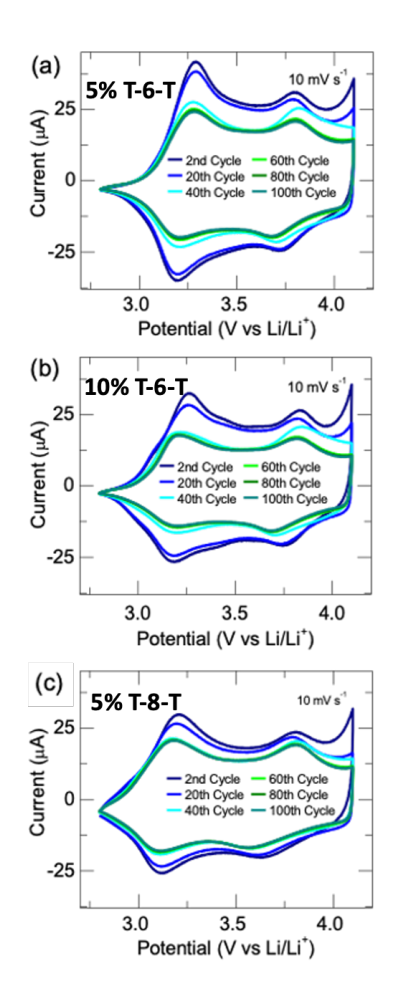


Figure 5. Long-term cycling at 10 mV $s^{\text{-}1}$ for (a) 5% T-6-T, (b) 10% T-6-T and (c) 5% T-8-T

Electronic and Ionic Conductivity of PProDOT-CBS Random Copolymers

Electronic Conductivity: To investigate the effect of CBS units on the electronic charge transport of PProDOT-CBS random copolymers, electronic conductivity of the polymer thin films was measured using electrochemical impedance spectroscopy (EIS) in 1 M LiTFSI in EC/DMC as a function of electrochemical potential. Conductivity of the polymers was measured using our previously established method,⁶⁸ that allows simultaneous determination of electronic and ionic conductivity as a function of electrochemical doping. **Fig. 6a** shows the

electronic conductivity of PProDOT-Hx2 and of all the PProDOT-CBS polymers as a function of electrode potential aside from 20% T-8-T and 20% T-10-T, which were not electrochemically active enough to obtain meaningful electronic conductivities. Fig. 6b shows the electronic conductivity of T-6-T copolymers as an illustration of the impact of increasing CBS content. At 2.9 V vs Li/Li⁺, the electronic conductivity of 5% T-6-T is 1.19×10⁻⁵ S cm⁻¹, which is 30× lower that PProDOT-Hx2. Upon doping, the electronic conductivity of 5% T-6-T increases to a maximum of 5×10⁻² S cm⁻¹ at 3.3 V. The electronic conductivity slightly decreases at higher voltages, likely due to increasing bipolaron formation, until reaching 9×10 ³ S cm⁻¹ at 3.7 V, and is then relatively constant above 3.7 V vs Li/Li⁺. Although a similar trend is observed with PProDOT-Hx2, its electronic conductivity reaches 1.06 S cm⁻¹, ~20× higher than 5% T-6-T. Upon increasing the content of T-6-T even further, the undoped electronic conductivity drops further to 2×10-6 S cm-1 and 1×10-6 S cm-1 for 10% and 20% T-6-T respectively. Upon doping, 10% T-6-T reaches a maximum conductivity of 1.9×10⁻⁴ S cm⁻¹ at 3.3 V, approximately four orders of magnitude lower than that of PProDOT-Hx2. The maximum electronic conductivity of 20% T-6-T is another magnitude lower reaching only $2.4{\times}10^{\text{-5}}~S~cm^{\text{-1}}$ at $3.3~V~vs~Li/Li^{\text{+}}.$

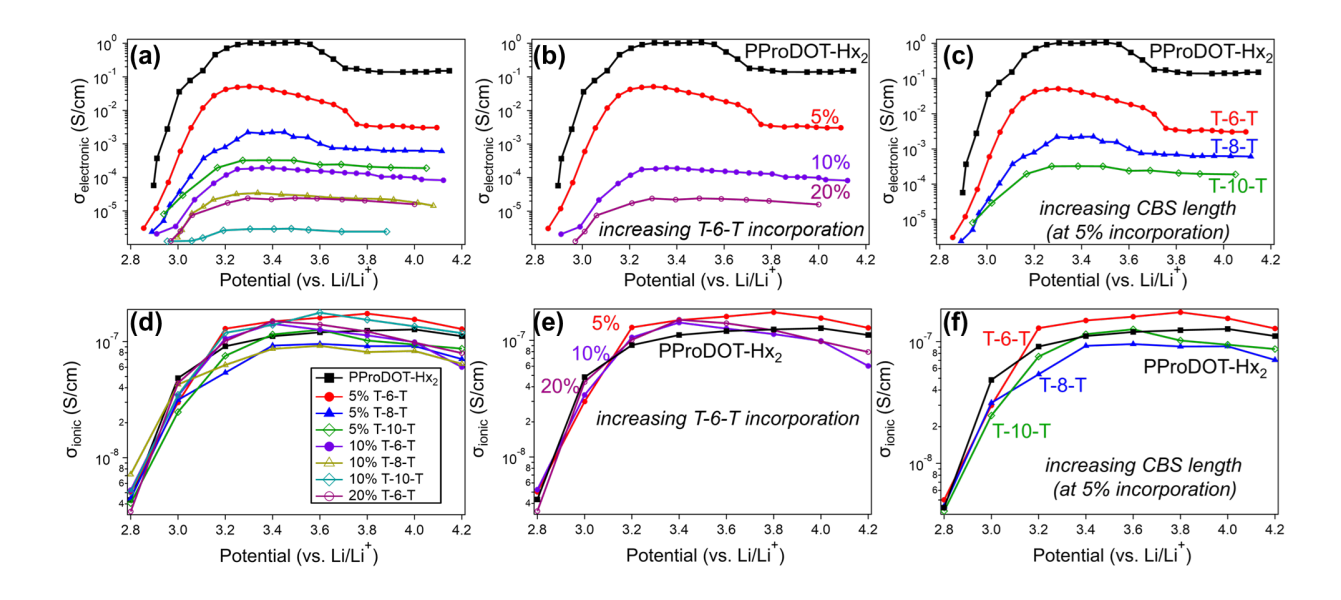


Figure 6. Electronic conductivities of (a) PProDOT-Hx2 and the electrochemically active PProDOT-CBS random copolymers, (b) 5%, 10%, and 20% T-6-T PProDOT-CBS random copolymers, demonstrating the effect of increasing CBS incorporation on the electronic conductivity while keeping the CBS length constant, (c) 5% T-6-T, 5% T-8-T, and 5% T-10-T PProDOT-CBS random copolymers, demonstrating the effect of increasing CBS length on the electronic conductivity while keeping the percentage of incorporation constant. Ionic conductivities of (d) PProDOT-Hx2 and the electrochemically active PProDOT-CBS random copolymers, (e) 5%, 10%, and 20% T-6-T PProDOT-CBS random copolymers, demonstrating the effect of increasing CBS incorporation on the ionic conductivity while keeping the CBS length constant, (f) 5% T-6-T, 5% T-8-T, and 5% T-10-T PProDOT-CBS random copolymers, demonstrating the effect of increasing CBS length on the ionic conductivity while keeping the percentage of incorporation constant.

A similar trend can be seen with the T-8-T and T-10-T PProDOT-CBS polymers where the electronic conductivity also decreases with increasing incorporation of CBS units, as shown in Fig. S34 and Fig. S35 respectively. The maximum electronic conductivity of 5% $(2.2 \times 10^{-3} \text{ S})$ cm⁻¹) and 10% T-8-T (3.4×10^{-5} S cm⁻¹) are three and five orders of magnitude lower than PProDOT-Hx₂, and in the T-10-T copolymer family, the decline in electronic conductivity is even more drastic, as the maximum electronic conductivity of 5% T-10-T is approximately four orders of magnitude lower than that of PProDOT-Hx2, at only 3.2 ×10⁻⁴ S cm⁻¹. These results clearly demonstrate the reduction in electronic charge transport properties of the PProDOT-CBS copolymers with increasing content of break spacer, a result which agrees well with the general trend in literature.⁶⁴ Fig. 6c shows the effect on the electronic conductivity when keeping the percentage of CBS incorporation constant and increasing the break spacer length. Upon introducing 5% T-6-T, the maximum electronic conductivity drops to 5×10^{-2} S/cm from 1.06 S/cm for PProDOT-Hx2. Increasing the chain length to 8 carbons reduces the maximum electronic conductivity even more to 2.2×10^{-3} S/cm. The 10-carbon CBS unit, T-10-T, further reduces the maximum electronic conductivity to 3.3×10^{-4} S/cm. Overall, we found that increasing either the incorporated content of CBS units or increasing the length of the CBS unit decreases the electronic charge transport ability of these conjugated polymers.

Ionic Conductivity: Interestingly, although the introduction of CBS units has a significant effect on the electronic transport properties of the conjugated polymers, the ionic conductivity as a function of electrochemical doping, shown in **Fig. 6d**, reveals a smaller impact of CBS

incorporation on ionic conductivity relative to PProDOT-Hx2. This can be explained by the fact that introduction of non-polar CBS spacers should not significantly change the ion-affinity or solvent swelling of the resulting PProDOT-CBS polymers. However, as shown in Fig. 6e, Fig. 6f and Table S2, just like the electronic conductivity, but at a much lesser extent, increasing either the incorporated amount of CBS units or increasing the length of the CBS units decreases the ionic conductivity. The 5% T-6-T has the highest ionic conductivity of the PProDOT-CBS polymers, and increasing either the length or incorporation leads to lower ion transport ability in these conjugated polymers. This likely arises for two reasons. First, the propylenedioxy group is polar and thus plays a meaningful role in coordinating Li⁺ in the film, facilitating ion transport.⁶⁹ In addition, solvent swelling is very important for Li⁺ transport. The CBS segments cannot be doped, and when the polymer backbone is doped, it becomes more polar, facilitating solvent swelling, and this effect helps give rise to the large increase in ionic conductivity observed upon electrochemical doping in Fig. 6d-f. Since doping cannot occur in the break-spacer regime of the PProDOT-CBS polymers, solvent swelling and ionic conductivity are both expected to be lower. However, it is worth mentioning that the 5% T-10-T polymer has a slightly increased ionic conductivity compared to 5% T-8-T (**Table S2**), but the fact remains that 5% T-6-T has the highest ionic conductivity of the series and ionic conductivity decreases by either increasing CBS length or incorporation.

Morphological Investigation of PProDOT-CBS Random Copolymers upon Electrochemical Doping

To understand the effect of CBS unit incorporation into the PProDOT-Hx2 backbone on the resulting PProDOT-CBS copolymers, in both the neutral and electrochemically doped forms, we performed grazing incidence wide-angle X-ray scattering (GIWAXS) to probe the morphology of the polymers. GIWAXS is a scattering technique used to provide information about the atomic and molecular distances in polymer crystallites and their orientation with respect to the substrate. GIWAXS allows us to examine structural differences between the PProDOT-CBS family and pure PProDOT-Hx2, in both doped and undoped forms. ^{26,34} Similar to what we have observed in our previous studies, ²⁶ all of the PProDOT-CBS polymers are quite disordered as deposited, characterized only by a lamellar (100) peak at $\sim 0.4 \, \text{Å}^{-1}$ and a π -stacking (010) peak at $\sim 1.4 \, \text{Å}^{-1}$. While the lamellar peak corresponds to the side chain spacing between the polymer chains, the π -stacking peak is correlated to the distance between polymer chains along the lattice vector closest to the π -stacking direction.

Fig. 7a shows the normalized fully integrated GIWAXS diffractograms of the three best electrochemically behaved polymers: 5% T-6-T (red), 10% T-6-T (purple) and 5% T-8-T (blue), all compared to PProDOT-Hx₂ (black). All of the diffraction patterns are normalized to their respective (020) π -stacking peaks. In literature, the π -stacking peak is often referred to as the (010) diffraction peak, but based on the unit cell symmetry, it should be referred to as the (020) instead.^{70,71} The neutral polymers are all fairly similar, shown by their similar 2D diffractograms in Figure S36a. The undoped T-6-T polymers have similar $q_{(100)}$ at $^{\sim}$ 0.40 Å⁻¹ (d-spacing = 15.7 Å), while the T-8-T polymer has a $q_{(100)}$ location of 0.36 Å⁻¹ (d-spacing = 17.5 Å),

showing that the break-spacer length has a slight effect on the lamellar distance of the polymer. Additionally, the 5% and 10% T-6-T also have similar FWHM, while the 5% T-8-T polymer has a wider FWHM. The FWHM of a diffraction peak can be used to calculate the coherence length (L) and/or the paracrystallinity disorder parameter (g), depending on the assumptions made. Coherence length can be calculated using the Scherrer equation, with the assumption that only crystallite size broadens the diffraction peaks. For semicrystalline materials, like conjugated polymers, however, paracrystalline disorder, amongst other microstructural distortions, can dominate peak broadening.⁷² The quality of our diffraction data is not sufficient so separate these two broadening mechanisms, but values can be readily calculated under the assumption that either effect dominates the peak broadening, as shown in Fig. S36b. In general, with increasing CBS length or incorporation, L decreases or g increases. Together, the changes in *L* and *g* show that increasing CBS length or incorporation leads to more disordered polymers. The trends in these values are most likely due to the longer conjugated break-spacer units and the fact that sp³ carbons are much less rigid than the sp² carbons in a conjugated system. 73 Upon doping, L increases or g decreases in all cases, but the changes in *L* and *g* are the largest in the 5% T-6-T, confirming that the 5% T-6-T polymer has the largest increase in structural ordering upon electrochemical doping.

Electrochemical doping of the PProDOT-CBS copolymers was carried out in a threeneck cell, where Li metal was the counter and the reference electrodes, and the polymer on Al-back-coated Si was the working electrode. The electrolyte consisted of 1 M LiTFSI in EC:DMC (1:1) (v/v). When electrochemically doped, the TFSI⁻ anion acts as the counterion to balance the polaronic charge within the polymer film. **Fig. 7b** shows 5% T-6-T (red trace), 5% T-8-T (blue trace), and 10% T-6-T (purple trace) when doped at 3.2 V vs. Li/Li⁺. At this potential, the dominant charged species are polarons. Previous work from our group has established that the crystallinity of PProDOTs increases dramatically upon electrochemical doping. Comparing all three polymers, the polymers with 5% CBS incorporated show larger increases in crystallinity upon electrochemical doping than the sample with 10% CBS. Within the 5% CBS polymers, the polymer with the shortest CBS unit, the 5% T-6-T, showed that largest increase in crystallinity upon electrochemical doping.

The GIWAXS patterns displayed in **Fig. 7c-e** show the three best performing CBS polymers, this time comparing the neutral, undoped diffraction pattern with patterns collected at multiple potentials to observe the evolution of structure with increasing doping level. Poorly crystalline materials tend to be poor conductors, and while the PProDOT-CBS polymers all start out rather amorphous, they all become more crystalline with electrochemical doping and stay more crystalline throughout the entire potential window of a cathode electrode. Specifically, upon doping at the lowest potentials, when polarons are the dominant charge species (3.2 vs. Li/Li⁺, lightest gray trace in Figures 7c-7e), the q_{100} peak shifts to lower position (larger size) as the structure rearranges to accommodate the TFSI⁻ anion in the polymer matrix. When doped, the 5% T-6-T and 5% T-8-T polymers shift to the same location for the q_{100} at 0.32 (d-spacing = 19.6 Å), while the 10% T-6-T shifts to the q_{100} at 0.34 (d-spacing = 18.5 Å).

Finally, **Fig. 7f** shows only the lamellar peak progression of the three PProDOT-CBS polymers doped to different potentials on the same y-axis to further demonstrate that the PProDOT-CBS polymer with the shortest and smallest incorporation of CBS units is best able to crystallize upon doping. Increasing percentage incorporation of CBS units disrupts the π conjugation, resulting in a loss of crystallinity and thereby a decline in conductivity (Fig. 6a). The enhanced conformational randomness is also evident in their lower tensile modulus and higher crack onset strain, discussed in the following section. Furthermore, keeping the percentage incorporation of spacer constant at 5% and increasing the spacer length from 6 to eight carbons also resulted in similar property changes. Overall, the final crystallinity after doping, as reflected in the GIWAXS peak intensity (Fig. 7f), correlates quite well with both the electronic conductivity data of the PProDOT-CBS polymers (Fig. 6) and mechanical measurements (Fig. 8 and Fig. 9), where we see that more crystalline materials are better electronic conductors, but less crystalline materials in general tend to be more ductile. We note, however, that in addition to different fractions and lengths of break spacers, there is another structural difference, which is the fact that the M_n of the polymers are not all the same. In particular, the 5% T-6-T polymer, which shows the largest increase in crystallinity upon electrochemical doping, is also the polymer with the highest Mn (37.2 kDa compared to 16 kDa and 15.9 kDa for 10% T-6-T and 5% T-8-T, respectively, and 17.4 kDa for ProDOT-Hx2). The higher molecular weight is not likely to be a dominant factor in the observed changes in crystallinity, as it is lower Mn that typically leads to more crystalline polymers, 74,75 but the

molecular weight differences can have a significant effect on the mechanical properties, as discussed in the next section.

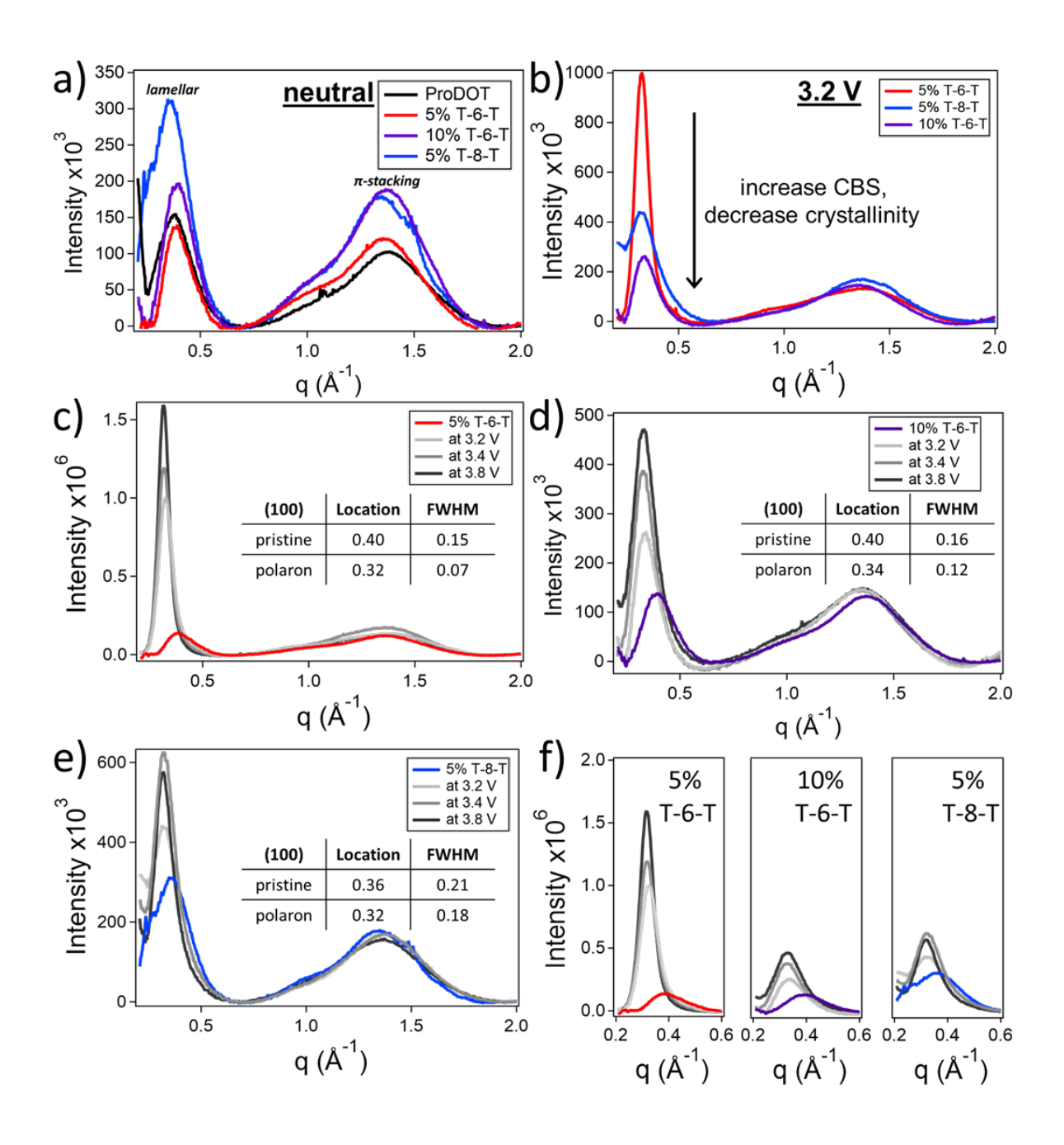


Figure 7. Radial integrations of a) neutral polymers, comparing PProDOT-Hx₂ to the PProDOT-CBS copolymers, with all patterns normalized to the π -stacking peak height, b) the

PProDOT-CBS copolymers doped at 3.2 V vs. Li/Li⁺, c) 5% T-6-T doped at 3.2 V (polaron), 3.4 V (bipolaron) and 3.8 V vs. Li/Li⁺, d) 10% T-6-T doped at 3.2 V (polaron), 3.4 V (bipolaron) and 3.8 V vs. Li/Li⁺, and e) 5% T-8-T doped at 3.2 V (polaron), 3.4 V (bipolaron) and 3.8 V vs. Li/Li⁺ . f) Direct comparison of the intensity changes in the (100) lamellar peak with doping for the three best performing PProDOT-CBS copolymers.

Investigation of Mechanical Properties of PProDOT-CBS Random Copolymers

Due to the observed superior electrochemical reversibility, 5% T-6-T, 10% T-6-T and 5% T-8-T, were also selected for mechanical and cell testing. To analyze the effect of incorporating CBS units into the PProDOT-Hx2 backbone on the mechanical properties of the resulting PProDOT-CBS copolymers, we utilized the established "film-on-water" method, developed by Kim *et al.*76 We have also developed a related method that we call the "film-on-solvent" method, wherein the film is floated on the solvent used to make the battery electrolytes (EC/DMC in this case), instead of water to better mimic the environment inside a lithium ion battery, where the polymer binder is swollen by the electrolyte. The film-on-water method is a standardized pull test method measuring the intrinsic mechanical properties of freestanding films, which enables the generation of stress-strain curve that can be used to extract mechanical parameters such as the tensile (Young's) modulus (E), extensibility or crack-onset strain (COS), and ultimate tensile strength (UTS), among others (Fig. S37a-d).

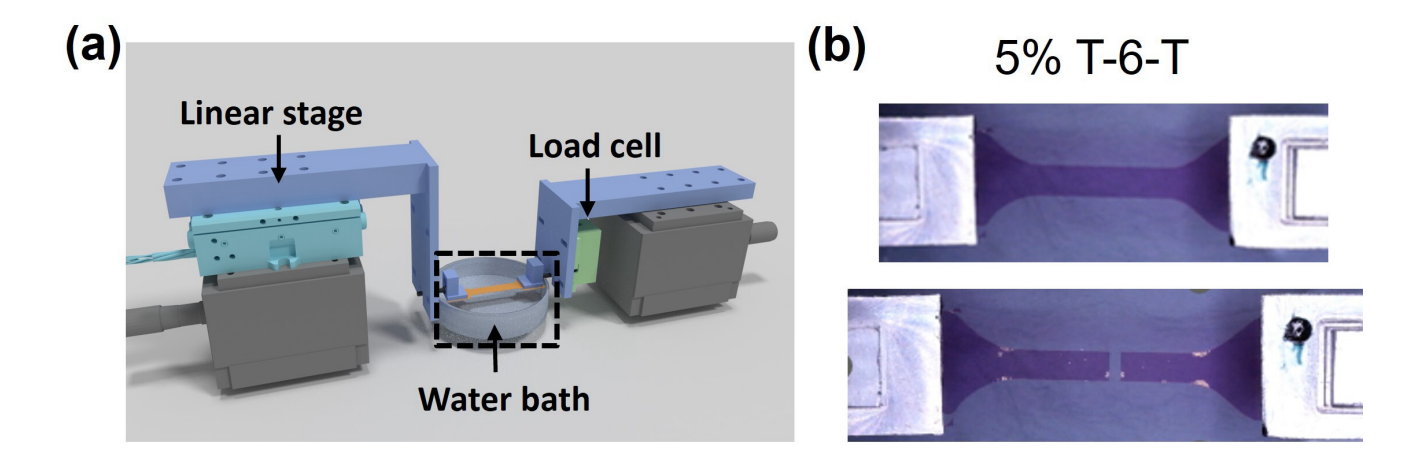


Figure 8. (a) The tensile testing system consisting of a load cell, a linear stage and water water/solvent bath on an anti-vibration table. Adapt with permission from reference XX (b) Optical image of a representative strained PProDOT-CBS polymer film. (c) Optical image of the representative strained PProDOT-CBS polymer film at failure.

Fig. 8a shows the set up for the tensile testing system, where a thin film of conducting polymer is floated on water and gradually stretched until it breaks (**Fig. 8b and 8c**). Additionally, for our newly developed film-on-solvent technique, we could also measure the mechanical properties of polymer thin films on top of electrolyte-mimic solution. In this case, the polymer thin film was first floated on water, followed by fast transfer to the solvent surface. We performed both of these experiments on the selected polymers, 5% T-6-T, 10% T-6-T, and 5% T-8-T, along with the fully conjugated reference polymer, PProDOT-Hx2 (**Fig. S38a-d and S39a-d**).

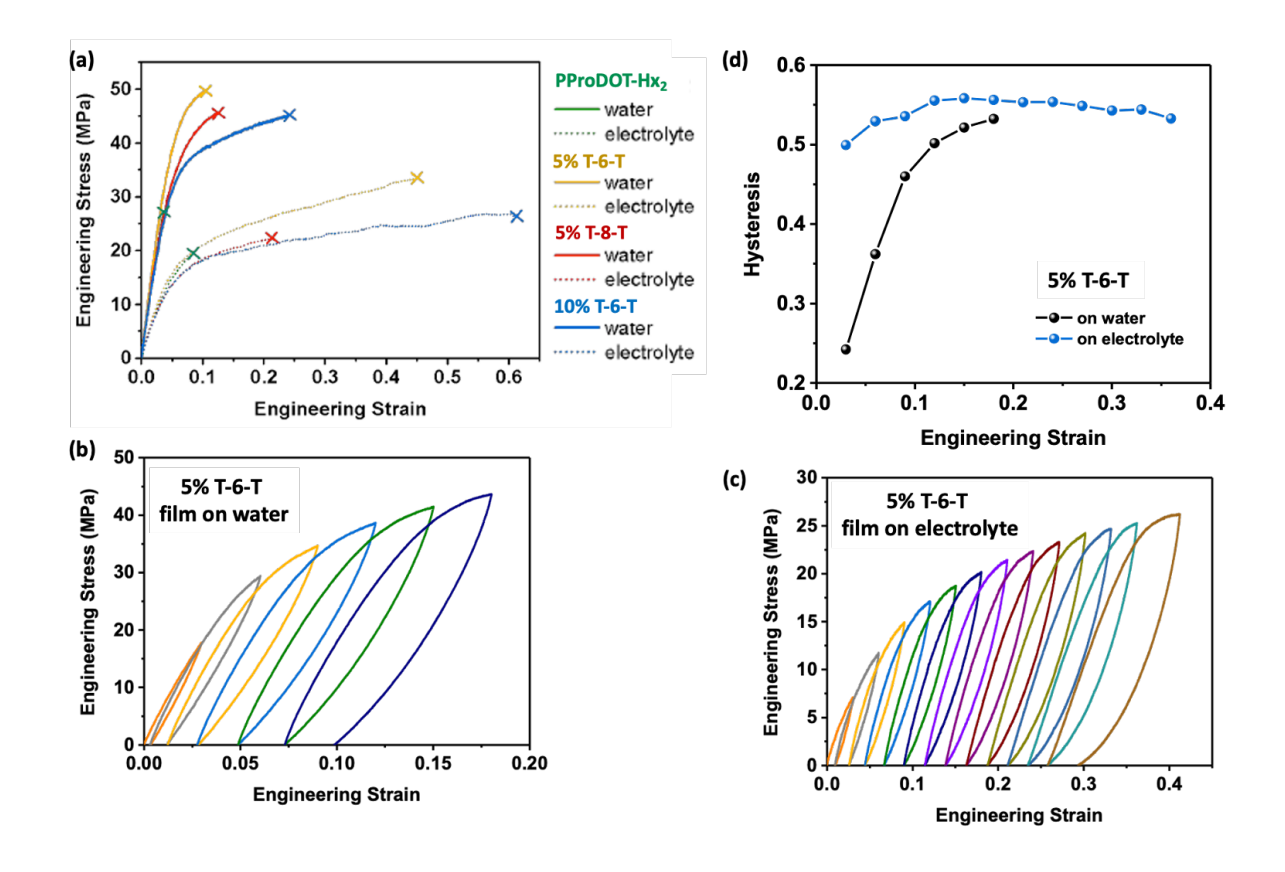


Figure 9. (a) Comparison of Stress–Strain curves for 5% T-6-T, 10% T-6-T, 5% T-8-T, and PProDOT-Hx₂ obtained using the film-on-water and film-on-solvent methodologies. (b) Hysteresis behavior of 5% T-6-T polymer film on water and (c) on solvent (EC/DMC 1:1). (d) Comparison of hysteresis behavior of 5% T-6-T polymer film on water and on solvent (EC/DMC 1:1).

A low value of Young's Modulus (E) and a high value of Crack Onset Strain (COS) are generally desired for a polymer to be stretchable or deformable, although this is not true always.⁷⁷ From the film-on-water data in **Fig. 9a** and **Table 1**, we observe that all three polymers have significantly higher COS (12-24%) compared to the fully conjugated PProDOT-Hx₂ (3.2%) and two of the three CBS polymers have lower modulus. This suggests that incorporation of CBS

units into the PProDOT backbone along with the random architecture, can induce ductility to the resulting polymers. The higher modulus observed for 5% T-6-T compared to PProDOT-Hx2 can be understood by remembering that the mechanical properties of polymer thin films dependent on the solid-state packing structure and not by the molecular/monomer structure alone.^{78,79} Hence, stiffness of polymer thin film cannot be exactly correlated to the chain stiffness or CBS fraction alone. Indeed, more ordered packing in the polymer thin film can produce greater stiffness and brittleness despite increased flexibility of the polymer backbone due to higher content of CBS incorporation, 65 and higher M_n polymer can improve the COS due to more chain entanglement.^{77,80} These two effects explain the mechanical behavior of the 5% T-6-T polymer, where E (5% T-6-T) > E (PProDOT-Hx₂), even though COS (5% T-6-T) > COS (PProDOT-Hx₂). In the case of 5% T-6-T, its higher molecular weight ($M_n = 37.2 \text{ kDa}$) compared to 13.2-19.3 kDa for the rest of the PProDOT-CBS copolymers (Table S1) and 17.4 kDa for PProDOT-Hx2 can contribute to both higher rigidity and higher strain at failure, because higher Mn polymers create a more interconnected network.

Table 1. Young's Modulus (E) and Crack Onset Strain (COS) of 5% T-6-T, 10% T-6-T, 5% T-8-T and PProDOT-Hx₂ obtained using both film-on-water and film-on-solvent (EC/DMC) methodologies.

	Film-On-	Film-On-	Film-On-	Film-On-
	Water	Water	Solvent	Solvent
Polymers	E (MPa)	COS (%)	E (MPa)	COS (%)
PProDOT-Hx2	858 ± 15	3.2 ± 0.6	434 ± 60	8.4 ± 1.5
5% T-6-T	980 ± 50	12 ± 3	479 ± 34	42 ± 6
5% T-8-T	849 ± 5	13 ± 2	398 ± 24	19 ± 9
10% T-6-T	784 ± 41	24 ± 5	420 ± 25	56 ± 17

The trend within the three PProDOT-CBS polymers aligns very well with the trend previously reported in the literature where tensile modulus and ductility not only depends on molecular flexibility but also on the solid-state packing structure.⁶⁵ By keeping the percentage incorporation of CBS unit constant and increasing the spacer length from 6 to 8 carbons i.e.,

moving from 5% T-6-T to 5% T-8-T, the tensile modulus, E, was found to decrease by $^{\sim}13.4\%$, while the COS increases by $^{\sim}13\%$. A similar trend was observed upon increasing the spacer content from 5% to 10% while keeping the spacer length constant at 6 carbons i.e., from 5% T-6-T to 10% T-6-T; in this case, E decreased by $^{\sim}$ 20% and the COS more than double its value ($^{\sim}$ 108% increase). This demonstrates that both higher content and increased length of CBS leads to a higher degree of ductility. We note that the order of magnitude of the tensile modulus of all the copolymers matches well with those of previously reported CBS copolymers ($^{<}$ 1 GPa).

For the PProDOT-CBS copolymers to be used as stretchable, conductive cathode binders in LIBs, the polymers are required to be immersed in the battery electrolyte, which is usually a mixture of polar organic solvents such as EC/DMC. Polymer binders almost always swell to some extent in the battery electrolyte, and such solvent-induced swelling plays a key role in the optimization of electronic and ionic conductivity in LIBs. ²⁶ This motivated us to investigate the trend in mechanical properties of thin films of PProDOT-CBS copolymers when floated on typical battery solvents, such as EC/DMC so as to understand the effect of solvent-induced swelling on their mechanical deformability and ductility. Indeed, we observed dramatic changes in the mechanical properties of 5% T-6-T, 10% T-6-T, 5% T-8-T and PProDOT-Hx2 using the film-on-solvent method as compared to the film-on-water method. The film-on-solvent data in Fig. 9a and Table 1 clearly shows that all of the films have lower modulus and higher COS when swollen with organic solvent comparted to the same films on water.

PProDOT-Hx2 showed a decrease in E from 858 MPa to 434 MPa and an increase in COS from 3.2% to 8.4%. Two out of the three PProDOT-CBS copolymers (5% T-8-T and 10% T-6-T) have both lower E and higher COS compared to PProDOT-Hx2. The 5% T-6-T is again an exception, where E is higher than that of PProDOT-Hx2 likely due to the higher Mn of 5% T-6-T and a more ordered packing in polymer thin film as described previously. However, the COS of the 5% T-6-T film is much higher than PProDOT-Hx2 (42% vs. 8.4%). Overall, the data suggest increased mechanical ductility and softness of the polymers in battery electrolyte, which can be ascribed to swelling of the polymer films by the organic solvent.

There is a noteworthy difference between the PProDOT-CBS polymers measured on water versus EC/DMC. Keeping CBS content fixed and increasing the CBS spacer length from 6 to 8 carbons, we observed that E (5% T-8-T) < E (5% T-6-T) for both solvents, but the failure strains (COS) were similar when measured on water, but very different when measured on organic solvent, with the 5% T-6-T showing a 2x higher value than the 5% T-8-T when measured on EC/DMC. E is a property of the elastic regime and COS is the strain at failure in the plastic regime of a stress-strain curve. We propose that this difference arises from the fact that increasing the spacer length from 6 to 8 carbons with insulating, non-polar alkyl chains should reduce the solvent swelling, thereby reducing the extensibility of the polymer in EC/DMC solvent. On the other hand, keeping the CBS spacer length constant and increasing the content from 5% to 10%, we observe that the trend is as expected, where E (10% T-6-T) < E (5% T-6-T) and COS (10% T-6-T) > COS (5% T-6-T). Interestingly, comparing film-on-water data with

film-on-solvent data, the enhancement in COS value observed for PProDOT-Hx $_2$ is \sim 2.6 times, 5% T-6-T is \sim 3.6 times, 5% T-8-T is \sim 1.4 times and 10% T-6-T is \sim 2.3 times.

The hysteresis behavior of PProDOT-CBS polymers was also studied on both water (Fig. 9b) and on solvent (EC/DMC 1:1) to mimic the electrolyte used in batteries, but without added salt (Fig. 9c) using 5% T-6-T for representative analysis, and hysteresis comparison of these two conditions is shown in Fig. 9d. The 5% T-6-T thin film showed higher hysteresis on solvent compared to on water, which is attributed to the higher swelling effect of 5% T-6-T in EC/DMC relative to water. This means that solvent has a more plasticizing effect on the polymer than water. In other words, PProDOT-CBS polymers are not elastic but rather plastic or more deformable. This aligns well with what we have observed in the stress-strain curves of these polymers characterized by a longer plastic regime and a smaller elastic regime. These results demonstrate that solvent in battery electrolyte plays an important role in the mechanical properties of polymer binders in LIBs.

Electrochemical Cycling of NCA Cathodes Using PProDOT-CBS as Polymer Binders

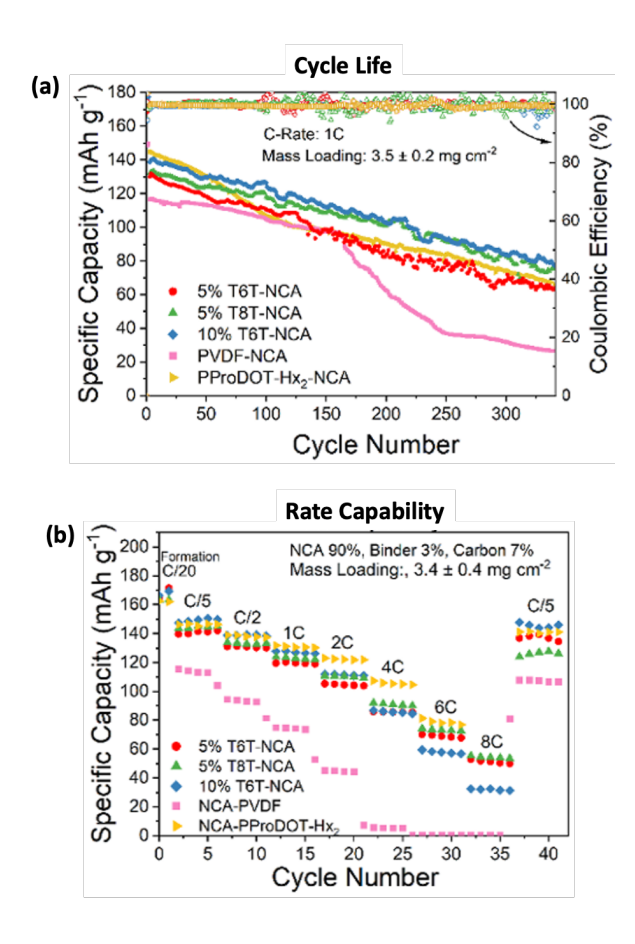


Figure 10. Long-term cycling and rate capability testing of the Li-NCA-PProDOT-CBS electrodes. (a) Specific capacity as a function of cycle number at constant charge/discharge rate of 1C and (b) Rate capability testing for the Li-NCA-5% T-6-T, Li-NCA-5% T-8-T, Li-NCA-10% T-6-T, Li-NCA-PProDOT-Hx₂, and Li-NCA-PVDF cells with a cathode mass composition of 90% NCA, 3% binder, and 7% carbon. Two formation cycles at C/20 were carried out before testing.

To investigate the efficiency of the PProDOT-CBS polymers as stretchable conductive cathode binders for LIBs, NCA cathodes employing 5% T-6-T, 5% T-8-T, 10% T-6-T as binders were cycled and compared against the fully conjugated reference PProDOT-Hx₂ and non-

conjugated PVDF. From the long-term cycling studies (**Fig. 10a**), we notice that when the electrodes are cycled at 1C for more than 300 cycles, all the PProDOT-CBS polymers and PProDOT-Hx2 retain much higher capacity as compared to PVDF. Furthermore, 10% T-6-T and 5% T-8-T retain higher capacity compared to PProDOT-Hx2 which is attributed to the higher COS and lower E values compared to PProDOT-Hx2 (**Fig. 9a** and **Table 1**), providing improved ductility. This clearly demonstrates the effect of CBS incorporation on the mechanical properties of polymer binders impacting their cycle life. The highest capacity retention of 10% T-6-T after 300 cycles aligns well with its highest COS of 56% (film-on-solvent) and therefore highest extensibility among the copolymer series.

To determine the discharge rate-capability, the electrode cells were charged at C/20 (two formation cycles), followed by discharging at various rates ranging from C/5 to 8C (Fig. 10b). We observed that in general, while all the conductive polymers have higher capacity retention at high rate compared to PVDF, polymers with higher electronic conductivity namely, PProDOT-Hx2, 5% T-6-T and 5% T-8-T (Fig. 6c) displayed higher capacity retention at high rates of discharge (2C to 8C). PProDOT-Hx2 consistently outperformed the PProDOT-CBS copolymers up to 6C owing to the highest electronic conductivity among all the polymers. The 10% T-6-T polymer showed the worst high-rate performance due to its poor electronic conductivity (Fig. 6c), which likely results from disruption of conjugation along the PProDOT backbone. This data suggests that there is a trade-off between stability and rate capability, and that co-optimization of electronic and mechanical properties is possible via strategic

introduction of conjugation break spacers, ultimately resulting in overall superior electrochemical performance. We conclude that while higher COS or extensibility and lower tensile modulus (E) plays a major role in long-term cycling stability, rate capability of composite electrodes depends on the effectiveness of electronic and ionic charge transport and hence on the conductivity of the polymer binders. For this study, these two values are best optimized in the 5% T-8-T polymer. A plot of the real part of the impedance response (Z_{re}) against frequency, galvanostatic charge-discharge curves for Fig. 10a, corresponding galvanostatic charge-discharge curves for Fig. 10b, and Nyquist plots as function of SOC in the first cycle after formation and after 400 cycles can all be found in the supporting information (Fig. S40-S44).

CONCLUSIONS:

A family of nine PProDOT-CBS random copolymers were synthesized via direct arylation polymerization (DArP), where conjugation break spacers (CBS, T-X-T) of varying spacer length (X = 6, 8, 10) and varying content (5%, 10% and 20%) were introduced into the conjugated PProDOT-Hx2 backbone to induce deformability to the resulting polymers, for use as stretchable, conductive cathode binders in LIBs. This is also the first report where CBS containing polymers have been synthesized via DArP. All nine copolymers were found to be insoluble in battery electrolyte and were investigated for their electrochemical and morphological properties and analyzed relative to the fully conjugated reference polymer PProDOT-Hx2. Electrochemical studies revealed that three out of the nine PProDOT-CBS

random copolymers i.e., 5% T-6-T, 5% T-8-T and 10% T-6-T showed good electrochemical reversibility and stability after 100 cycles. Their rapid kinetics and the high electrochemical reversibility of the doping process up to 100 mV s⁻¹ is facilitated by fast electron and ion transport, making these polymers suitable for conductive cathode binder for use in LIBs.

Electronic and ionic conductivity of all the PProDOT-CBS random copolymers aligned well with GIWAXS studies. While all polymers become more crystalline upon electrochemical doping, the extent of increase varied with the length and fraction of CBS incorporated. Using the intensity of the (100) lamellar diffraction peak to quantify the crystallinity, we found that the crystallinity of the doped polymers decreased with increasing CBS length ((100)5% T-10-T < $(100)_{5\% \text{ T-8-T}} < (100)_{5\% \text{ T-6-T}}$, as well as with increase in percentage incorporation of CBS ((100)_{20%} T-6-T < (100)10% T-6-T < (100)5% T-6-T). This is reflected in the electronic conductivity data of PProDOT-CBS copolymers, where we observe a sharp decline in electronic conductivity with increase in CBS spacer length and content, i.e $\sigma_{\text{electronic}}(20\% \text{ T-6-T}) < \sigma_{\text{electronic}}(10\% \text{ T-6-T}) <$ $\sigma_{\text{electronic}}(5\% \text{ T-6-T}) < PProDOT-Hx2 \text{ and } \sigma_{\text{electronic}}(5\% \text{ T-10-T}) < \sigma_{\text{electronic}}(5\% \text{ T-8-T}) < \sigma_{\text{electronic}$ T-6-T) < PProDOT-Hx2. In contrast, no significant differences were observed in the ionic conductivity of the doped PProDOT-CBS polymers compared to PProDOT-Hx2. Based on the electrochemical reversibility, stability over 100 cycles and electronic conductivity data, 5% T-6-T, 5% T-8-T, and 10% T-6-T were selected for further mechanical characterization and cell testing with NCA cathodes.

To examine the effect of CBS incorporation on the mechanical properties of PProDOT-CBS polymers, the well-established film-on-water and a new film-on-solvent method were used. In general, we observe that the tensile modulus (E) decreases, and crack onset strain (COS) increases with increase in CBS spacer length and content and relative to fully conjugated PProDOT-Hx2, confirming the fact that introduction of CBS can induce stretchability to PProDOT-based polymer binders. An exception was noticed in the case of 5% T-6-T where E (5% T-6-T) > E (PProDOT-Hx₂) although COS (5% T-6-T) > COS (PProDOT-Hx₂). This is attributed likely to the higher packing order in polymer thin film of the 5% T-6-T polymer. We also observe significant differences in the mechanical properties measured via the filmon-solvent method, where values of E are much lower and that of COS are much higher compared to the corresponding values obtained from film-on-water, where the difference is attributed to solvent swelling by the EC/DMC solvent. The improved ductility of the polymers in battery solvent is also confirmed by hysteresis studies of the 5% T-6-T polymer, wherein the stress-strain curves with increasing cyclic strains showed greater residual strain upon strain removal for film-on-water cycling compared to film-on-solvent testing. The highest COS was achieved for 10% T-6-T and lowest E was obtained for 5% T-8-T from the film-on-solvent data which aligned well with the battery performance with NCA cathodes.

Finally, to investigate the effect of stretchability introduced via CBS incorporation, cell testing with NCA cathodes was carried out for 5% T-6-T, 5% T-8-T and 10% T-6-T and analyzed relative to PProDOT-Hx2 and PVDF. Results from long-term cycling studies showed superior

performance with highest capacity retention after 300 cycles for the 10% T-6-T and 5% T-8-T polymers. A rate capability study showcased the importance of electronic conductivity over the mechanical properties of the polymer binders, where higher retention of capacity was observed for polymers with higher electronic conductivity. At the highest rates of discharge (8C), the 5% T-8-T and 5% T-6-T polymers exhibited the best performance, emphasizing that judicious introduction of CBS units can lead to co-optimization of electronic and mechanical properties, thereby resulting in enhanced electrochemical performance. The results presented clearly demonstrate that strategic introduction of conjugation break spacers into conjugated polymer binders is a viable approach towards stretchable conductive polymer binders for emerging high-capacity electrodes in LIBs.

ASSOCIATED CONTENT

Supporting Information

All monomer and polymer synthesis, NMR characterization, GPC traces of the PProDOT-CBS random copolymers, electrochemical testing method and cell fabrication, conductivity measurement technique, raw GIWAXS data of all the polymers, pseudo-free-standing thin-film tensile testing, electrode fabrication and cell assembly, impedance, galvanostatic charge-

discharge curves and 3D chart of impedance as a function of state of charge can be found in

the supporting information (PDF).

AUTHOR INFORMATION

Corresponding Authors

Barry C. Thompson – Department of Chemistry and Loker Hydrocarbon Research Institute,

University of Southern California, Los Angeles, California 90089-1661, United States.

Email: barrycth@usc.edu

Sarah H. Tolbert – Department of Chemistry and Biochemistry and Department of Materials

Science and Engineering, UCLA, Los Angeles, California 90095, USA.

Email: tolbert@chem.ucla.edu

Author Contributions

The manuscript was written through contributions of all authors. All authors have given

approval to the final version of the manuscript.

*P.D. and C.Z.S. contributed equally to this work.

^S.R.N. deceased.

Notes

The authors declare no competing financial interest.

43

FUNDING

This work was supported by the Center for Synthetic Control Across Length-Scales for Advancing Rechargeables (SCALAR), an Energy Frontier Research Center funded by the U. S. Department of Energy, Office of Science, Basic Energy Sciences under Award #DE-SC0019381. Use of the Stanford Synchrotron Radiation Lightsource, SLAC National Accelerator Laboratory, is supported by the U.S. Department of Energy, Office of Science, Office of Basic Energy Sciences under Contract No. DE-AC02-76SF00515. Y.W. and X. G. acknowledge funding from the NSF (DMR-2047689).

ACKNOWLEDGMENTS

The authors thank Professor Rachel A. Segalman and Gordon Pace for assistance with GPC measurements.

REFERENCES

- (1) Li, M.; Lu, J.; Chen, Z.; Amine, K. 30 Years of Lithium-Ion Batteries. *Advanced Materials* **2018**, *30* (33), 1800561. https://doi.org/10.1002/adma.201800561.
- (2) Kang, K.; Meng, Y. S.; Bre ger, J.; Grey, C. P.; Ceder, G. Electrodes with High Power and High Capacity for Rechargeable Lithium Batteries. *Science* **2006**, 311, 977-980. https://doi.org/10.1126/science.1122152.
- (3) Van der Ven, A.; Marianetti, C.; Morgan, D.; Ceder, G. Phase transformations and volume changes in spinel Li_xMn₂O₄. *Solid State Ionics* **2000**, 135, 21–32. https://doi.org/10.1016/S0167-2738(00)00326-X.
- (4) Li, Y.; Lu, J.; Wang, Z.; Wang, X.; Yuan, H.; Qin, N.; Yi, Z.; Chen, Z.; Gu, S.; Lu, Z. Suppressing Continuous Volume Expansion of Si Nanoparticles by an Artificial Solid Electrolyte Interphase for High-Performance Lithium-Ion Batteries. *ACS Sustainable Chem. Eng.* **2021**, *9* (24), 8059–8068. https://doi.org/10.1021/acssuschemeng.0c08964.

- (5) Hsieh, C.-C.; Lin, Y.-G.; Chiang, C.-L.; Liu, W.-R. Carbon-coated porous Si/C composite anode materials via two-step etching/coating processes for lithium-ion batteries. *Ceram. Int.* **2020**, 46, 26598–26607. https://doi.org/10.1016/j.ceramint.2020.07.128.
- (6) Dou, F.; Shi, L.; Chen, G.; Zhang, D. Silicon/Carbon Composite Anode Materials for Lithium-Ion Batteries. *Electrochem. Energ. Rev.* 2019, 2 (1), 149–198. https://doi.org/10.1007/s41918-018-00028-w.
- (7) Loveridge, M. J.; Lain, M. J.; Johnson, I. D.; Roberts, A.; Beattie, S. D.; Dashwood, R.; Darr, J. A.; Bhagat, R. Towards High Capacity Li-Ion Batteries Based on Silicon-Graphene Composite Anodes and Sub-Micron V-Doped LiFePO4 Cathodes. *Sci Rep* **2016**, *6* (1), 37787. https://doi.org/10.1038/srep37787.
- (8) Cui, L.-F.; Yang, Y.; Hsu, C.-M.; Cui, Y. Carbon–Silicon Core–Shell Nanowires as High Capacity Electrode for Lithium Ion Batteries. *Nano Lett.* **2009**, *9* (9), 3370–3374. https://doi.org/10.1021/nl901670t.
- (9) Jain, R.; Lakhnot, A. S.; Bhimani, K.; Sharma, S.; Mahajani, V.; Panchal, R. A.; Kamble, M.; Han, F.; Wang, C.; Koratkar, N. Nanostructuring versus Microstructuring in Battery Electrodes. *Nat Rev Mater* **2022**. https://doi.org/10.1038/s41578-022-00454-9.
- (10) Luo, W.; Fang, C.; Zhang, X.; Liu, J.; Ma, H.; Zhang, G.; Liu, Z.; Li, X. In Situ Generated Carbon Nanosheet-Covered Micron-Sized Porous Si Composite for Long-Cycling Life Lithium-Ion Batteries. *ACS Appl. Energy Mater.* **2021**, *4* (1), 535–544. https://doi.org/10.1021/acsaem.0c02445.
- (11) Long, J. W.; Dunn, B.; Rolison, D. R.; White, H. S. 3D Architectures for Batteries and Electrodes. *Advanced Energy Materials* **2020**, *10* (46), 2002457. https://doi.org/10.1002/aenm.202002457.
- (12) Sun, H.; Zhu, J.; Baumann, D.; Peng, L.; Xu, Y.; Shakir, I.; Huang, Y.; Duan, X. Hierarchical 3D Electrodes for Electrochemical Energy Storage. *Nat Rev Mater* **2019**, *4* (1), 45–60. https://doi.org/10.1038/s41578-018-0069-9.
- (13) Haag, J. M.; Pattanaik, G.; Durstock, M. F. Nanostructured 3D Electrode Architectures for High-Rate Li-Ion Batteries. *Advanced Materials* **2013**, *25* (23), 3238–3243. https://doi.org/10.1002/adma.201205079.
- (14) Jia, H.; Li, X.; Song, J.; Zhang, X.; Luo, L.; He, Y.; Li, B.; Cai, Y.; Hu, S.; Xiao, X.; Wang, C.; Rosso, K. M.; Yi, R.; Patel, R.; Zhang, J.-G. Hierarchical Porous Silicon Structures with Extraordinary Mechanical Strength as High-Performance Lithium-Ion Battery Anodes. *Nat Commun* **2020**, *11* (1), 1474. https://doi.org/10.1038/s41467-020-15217-9.
- (15) The Impact of Non-uniform Metal Scaffolds on the Performance of 3D Structured Silicon Anodes / Elsevier Enhanced Reader. https://doi.org/10.1016/j.est.2020.101502.
- (16) An, Y.; Wood, B. C.; Ye, J.; Chiang, Y.-M.; Wang, Y. M.; Tang, M.; Jiang, H. Mitigating Mechanical Failure of Crystalline Silicon Electrodes for Lithium Batteries by Morphological Design. *Phys. Chem. Chem. Phys.* **2015**, *17* (27), 17718–17728. https://doi.org/10.1039/C5CP01385B.
- (17) Chen, H.; Ling, M.; Hencz, L.; Ling, H. Y.; Li, G.; Lin, Z.; Liu, G.; Zhang, S. Exploring Chemical, Mechanical, and Electrical Functionalities of Binders for Advanced Energy-

- Storage Devices. *Chem. Rev.* **2018**, *118* (18), 8936–8982. https://doi.org/10.1021/acs.chemrev.8b00241.
- (18) Chen, J.; Liu, J.; Qi, Y.; Sun, T.; Li, X. Unveiling the Roles of Binder in the Mechanical Integrity of Electrodes for Lithium-Ion Batteries. *J. Electrochem. Soc.* **2013**, *160* (9), A1502–A1509. https://doi.org/10.1149/2.088309jes.
- (19) Cho, K. Y.; Kwon, Y. I.; Youn, J. R.; Song, Y. S. Interaction Analysis between Binder and Particles in Multiphase Slurries. *Analyst* **2013**, *138* (7), 2044. https://doi.org/10.1039/c3an36720g.
- (20) Chen, Z.; Christensen, L.; Dahn, J. R. Comparison of PVDF and PVDF-TFE-P as Binders for Electrode Materials Showing Large Volume Changes in Lithium-Ion Batteries. *J. Electrochem. Soc.* **2003**, *150* (8), A1073. https://doi.org/10.1149/1.1586922.
- (21) Lingappan, N.; Kong, L.; Pecht, M. The Significance of Aqueous Binders in Lithium-Ion Batteries. *Renewable and Sustainable Energy Reviews* **2021**, *147*, 111227. https://doi.org/10.1016/j.rser.2021.111227.
- (22) Li, J.-T.; Wu, Z.-Y.; Lu, Y.-Q.; Zhou, Y.; Huang, Q.-S.; Huang, L.; Sun, S.-G. Water Soluble Binder, an Electrochemical Performance Booster for Electrode Materials with High Energy Density. *Advanced Energy Materials* **2017**, *7* (24), 1701185. https://doi.org/10.1002/aenm.201701185.
- (23) Yang, Y.; Wu, S.; Zhang, Y.; Liu, C.; Wei, X.; Luo, D.; Lin, Z. Towards Efficient Binders for Silicon Based Lithium-Ion Battery Anodes. *Chemical Engineering Journal* **2021**, *406*, 126807. https://doi.org/10.1016/j.cej.2020.126807.
- (24) Nguyen, V. A.; Kuss, C. Review—Conducting Polymer-Based Binders for Lithium-Ion Batteries and Beyond. *J. Electrochem. Soc.* **2020**, *167* (6), 065501. https://doi.org/10.1149/1945-7111/ab856b.
- (25) Wu, M.; Xiao, X.; Vukmirovic, N.; Xun, S.; Das, P. K.; Song, X.; Olalde-Velasco, P.; Wang, D.; Weber, A. Z.; Wang, L.-W.; Battaglia, V. S.; Yang, W.; Liu, G. Toward an Ideal Polymer Binder Design for High-Capacity Battery Anodes. *J. Am. Chem. Soc.* **2013**, *135* (32), 12048–12056. https://doi.org/10.1021/ja4054465.
- (26) Das, P.; Elizalde-Segovia, R.; Zayat, B.; Salamat, C. Z.; Pace, G.; Zhai, K.; Vincent, R. C.; Dunn, B. S.; Segalman, R. A.; Tolbert, S. H.; Narayan, S. R.; Thompson, B. C. Enhancing the Ionic Conductivity of Poly(3,4-Propylenedioxythiophenes) with Oligoether Side Chains for Use as Conductive Cathode Binders in Lithium-Ion Batteries. *Chem. Mater.* **2022**, *34* (6), 2672–2686. https://doi.org/10.1021/acs.chemmater.1c03971.
- (27) Hwang, C.; Lee, J.; Jeong, J.; Lee, E.; Kim, J.; Kim, S.; Yang, C.; Song, H.-K. The Rational Design of a Redox-Active Mixed Ion/Electron Conductor as a Multi-Functional Binder for Lithium-Ion Batteries. *J. Mater. Chem. A* **2021**, *9* (8), 4751–4757. https://doi.org/10.1039/D0TA08913C.
- (28) Zeng, W.; Wang, L.; Peng, X.; Liu, T.; Jiang, Y.; Qin, F.; Hu, L.; Chu, P. K.; Huo, K.; Zhou, Y. Enhanced Ion Conductivity in Conducting Polymer Binder for High-Performance Silicon Anodes in Advanced Lithium-Ion Batteries. *Advanced Energy Materials* **2018**, *8* (11), 1702314. https://doi.org/10.1002/aenm.201702314.

- (29) Wang, L.; Liu, T.; Peng, X.; Zeng, W.; Jin, Z.; Tian, W.; Gao, B.; Zhou, Y.; Chu, P. K.; Huo, K. Highly Stretchable Conductive Glue for High-Performance Silicon Anodes in Advanced Lithium-Ion Batteries. *Advanced Functional Materials* **2018**, *28* (3), 1704858. https://doi.org/10.1002/adfm.201704858.
- (30) Carboxymethyl chitosan/conducting polymer as water-soluble composite binder for LiFePO4 cathode in lithium ion batteries / Elsevier Enhanced Reader. https://doi.org/10.1016/j.jpowsour.2016.10.041.
- (31) An, H.; Li, X.; Chalker, C.; Stracke, M.; Verduzco, R.; Lutkenhaus, J. L. Conducting Block Copolymer Binders for Carbon-Free Hybrid Vanadium Pentoxide Cathodes with Enhanced Performance. *ACS Appl. Mater. Interfaces* **2016**, *8* (42), 28585–28591. https://doi.org/10.1021/acsami.6b08028.
- (32) Javier, A. E.; Patel, S. N.; Hallinan Jr., D. T.; Srinivasan, V.; Balsara, N. P. Simultaneous Electronic and Ionic Conduction in a Block Copolymer: Application in Lithium Battery Electrodes. *Angewandte Chemie International Edition* **2011**, *50* (42), 9848–9851. https://doi.org/10.1002/anie.201102953.
- (33) Patel, S. N.; Javier, A. E.; Balsara, N. P. Electrochemically Oxidized Electronic and Ionic Conducting Nanostructured Block Copolymers for Lithium Battery Electrodes. *ACS Nano* **2013**, *7*(7), 6056–6068. https://doi.org/10.1021/nn4018685.
- (34) Das, P.; Zayat, B.; Wei, Q.; Salamat, C. Z.; Magdău, I.-B.; Elizalde-Segovia, R.; Rawlings, D.; Lee, D.; Pace, G.; Irshad, A.; Ye, L.; Schmitt, A.; Segalman, R. A.; Miller, T. F.; Tolbert, S. H.; Dunn, B. S.; Narayan, S. R.; Thompson, B. C. Dihexyl-Substituted Poly(3,4-Propylenedioxythiophene) as a Dual Ionic and Electronic Conductive Cathode Binder for Lithium-Ion Batteries. *Chem. Mater.* **2020**, *32* (21), 9176–9189. https://doi.org/10.1021/acs.chemmater.0c02601.
- (35) Su, Y.; Feng, X.; Zheng, R.; Lv, Y.; Wang, Z.; Zhao, Y.; Shi, L.; Yuan, S. Binary Network of Conductive Elastic Polymer Constraining Nanosilicon for a High-Performance Lithium-Ion Battery. *ACS Nano* **2021**, *15* (9), 14570–14579. https://doi.org/10.1021/acsnano.1c04240.
- (36) Chen, S.; Song, Z.; Wang, L.; Chen, H.; Zhang, S.; Pan, F.; Yang, L. Establishing a Resilient Conductive Binding Network for Si-Based Anodes via Molecular Engineering. *Acc. Chem. Res.* **2022**, *55* (15), 2088–2102. https://doi.org/10.1021/acs.accounts.2c00259.
- (37) Kim, J.; Kim, M.-S.; Lee, Y.; Kim, S.-Y.; Sung, Y.-E.; Ko, S. H. Hierarchically Structured Conductive Polymer Binders with Silver Nanowires for High-Performance Silicon Anodes in Lithium-Ion Batteries. *ACS Appl. Mater. Interfaces* **2022**, *14* (15), 17340–17347. https://doi.org/10.1021/acsami.2c00844.
- (38) Chen, Z.; To, J. W. F.; Wang, C.; Lu, Z.; Liu, N.; Chortos, A.; Pan, L.; Wei, F.; Cui, Y.; Bao, Z. A Three-Dimensionally Interconnected Carbon Nanotube–Conducting Polymer Hydrogel Network for High-Performance Flexible Battery Electrodes. *Advanced Energy Materials* **2014**, *4* (12), 1400207. https://doi.org/10.1002/aenm.201400207.

- (39) Wu, H.; Yu, G.; Pan, L.; Liu, N.; McDowell, M. T.; Bao, Z.; Cui, Y. Stable Li-Ion Battery Anodes by in-Situ Polymerization of Conducting Hydrogel to Conformally Coat Silicon Nanoparticles. *Nat Commun* **2013**, *4*(1), 1943. https://doi.org/10.1038/ncomms2941.
- (40) Nam, J.; Kim, E.; K.K., R.; Kim, Y.; Kim, T.-H. A Conductive Self Healing Polymeric Binder Using Hydrogen Bonding for Si Anodes in Lithium Ion Batteries. *Sci Rep* **2020**, *10* (1), 14966. https://doi.org/10.1038/s41598-020-71625-3.
- (41) Zhao, Y.-M.; Yue, F.-S.; Li, S.-C.; Zhang, Y.; Tian, Z.-R.; Xu, Q.; Xin, S.; Guo, Y.-G. Advances of Polymer Binders for Silicon-Based Anodes in High Energy Density Lithium-Ion Batteries. *InfoMat* **2021**, *3*(5), 460–501. https://doi.org/10.1002/inf2.12185.
- (42) Liu, X.; Xu, Z.; Iqbal, A.; Chen, M.; Ali, N.; Low, C.; Qi, R.; Zai, J.; Qian, X. Chemical Coupled PEDOT:PSS/Si Electrode: Suppressed Electrolyte Consumption Enables Long-Term Stability. *Nano-Micro Lett.* **2021**, *13* (1), 54. https://doi.org/10.1007/s40820-020-00564-5.
- (43) Tang, R.; Ma, L.; Zhang, Y.; Zheng, X.; Shi, Y.; Zeng, X.; Wang, X.; Wei, L. A Flexible and Conductive Binder with Strong Adhesion for High Performance Silicon-Based Lithium-Ion Battery Anode. *ChemElectroChem* **2020**, *7* (9), 1992–2000. https://doi.org/10.1002/celc.201902152.
- (44) Yan, H.; Arima, S.; Mori, Y.; Kagata, T.; Sato, H.; Okuzaki, H. Poly(3,4ethylenedioxythiophene)/poly(4-styrenesulfonate): Correlation colloidal between and thin films. Thin Solid *Films* 2009. 517, 3299-3303. particles https://doi.org/10.1016/j.tsf.2009.01.004.
- (45) Ding, Z.; Liu, D.; Zhao, K.; Han, Y. Optimizing Morphology to Trade Off Charge Transport and Mechanical Properties of Stretchable Conjugated Polymer Films. *Macromolecules* **2021**, *54*(9), 3907–3926. https://doi.org/10.1021/acs.macromol.1c00268.
- (46) Printz, A. D.; Lipomi, D. J. Competition between Deformability and Charge Transport in Semiconducting Polymers for Flexible and Stretchable Electronics. *Applied Physics Reviews* **2016**, *3*(2), 021302. https://doi.org/10.1063/1.4947428.
- (47) Root, S. E.; Savagatrup, S.; Printz, A. D.; Rodriquez, D.; Lipomi, D. J. Mechanical Properties of Organic Semiconductors for Stretchable, Highly Flexible, and Mechanically Robust Electronics. *Chem. Rev.* **2017**, *117* (9), 6467–6499. https://doi.org/10.1021/acs.chemrev.7b00003.
- (48) O'Connor, T. F.; Rajan, K. M.; Printz, A. D.; Lipomi, D. J. Toward Organic Electronics with Properties Inspired by Biological Tissue. *J. Mater. Chem. B* **2015**, *3* (25), 4947–4952. https://doi.org/10.1039/C5TB00173K.
- (49) Xu, J.; Wang, S.; Wang, G.-J. N.; Zhu, C.; Luo, S.; Jin, L., *et al.*, Highly stretchable polymer semiconductor films through the nanoconfinement effect. *Science* **2017**, 355, 59-64. https://doi.org/10.1126/science.aah4496.
- (50) Zhang, G.; McBride, M.; Persson, N.; Lee, S.; Dunn, T. J.; Toney, M. F.; Yuan, Z.; Kwon, Y.-H.; Chu, P.-H.; Risteen, B.; Reichmanis, E. Versatile Interpenetrating Polymer Network Approach to Robust Stretchable Electronic Devices. *Chem. Mater.* **2017**, *29*(18), 7645–7652. https://doi.org/10.1021/acs.chemmater.7b03019.

- (51) Chiang, Y.-C.; Shih, C.-C.; Tung, S.-H.; Chen, W.-C. Blends of polythiophene nanowire/fluorine rubber with multiscale phase separation suitable for stretchable semiconductors. *Polymer* **2018**, 155, 146–151. https://doi.org/10.1016/j.polymer.2018.09.044.
- (52) Ditte, K.; Perez, J.; Chae, S.; Hambsch, M.; Al-Hussein, M.; Komber, H.; Formanek, P.; Mannsfeld, S. C. B.; Fery, A.; Kiriy, A.; Lissel, F. Ultrasoft and High-Mobility Block Copolymers for Skin-Compatible Electronics. *Advanced Materials* **2021**, *33* (4), 2005416. https://doi.org/10.1002/adma.202005416.
- (53) Mun, J.; Wang, G.-J. N.; Oh, J. Y.; Katsumata, T.; Lee, F. L.; Kang, J.; Wu, H.-C.; Lissel, F.; Rondeau-Gagné, S.; Tok, J. B.-H.; Bao, Z. Effect of Nonconjugated Spacers on Mechanical Properties of Semiconducting Polymers for Stretchable Transistors. *Advanced Functional Materials* **2018**, *28* (43), 1804222. https://doi.org/10.1002/adfm.201804222.
- (54) Galuska, L. A.; McNutt, W. W.; Qian, Z.; Zhang, S.; Weller, D. W.; Dhakal, S.; King, E. R.; Morgan, S. E.; Azoulay, J. D.; Mei, J.; Gu, X. Impact of Backbone Rigidity on the Thermomechanical Properties of Semiconducting Polymers with Conjugation Break Spacers. *Macromolecules* **2020**, *53* (14), 6032–6042. https://doi.org/10.1021/acs.macromol.0c00889.
- (55) Wu, Y.-S.; Lin, Y.-C.; Hung, S.-Y.; Chen, C.-K.; Chiang, Y.-C.; Chueh, C.-C.; Chen, W.-C. Investigation of the Mobility–Stretchability Relationship of Ester-Substituted Polythiophene Derivatives. *Macromolecules* **2020**, *53* (12), 4968–4981. https://doi.org/10.1021/acs.macromol.0c00193.
- (56) Chiang, Y.-C.; Wu, H.-C.; Wen, H.-F.; Hung, C.-C.; Hong, C.-W.; Kuo, C.-C.; Higashihara, T.; Chen, W.-C. Tailoring Carbosilane Side Chains toward Intrinsically Stretchable Semiconducting Polymers. *Macromolecules* **2019**, *52* (11), 4396–4404. https://doi.org/10.1021/acs.macromol.9b00589.
- (57) Wang, G.-J. N.; Shaw, L.; Xu, J.; Kurosawa, T.; Schroeder, B. C.; Oh, J. Y.; Benight, S. J.; Bao, Z. Inducing Elasticity through Oligo-Siloxane Crosslinks for Intrinsically Stretchable Semiconducting Polymers. *Advanced Functional Materials* **2016**, *26* (40), 7254–7262. https://doi.org/10.1002/adfm.201602603.
- (58) Zheng, Y.; Ashizawa, M.; Zhang, S.; Kang, J.; Nikzad, S.; Yu, Z.; Ochiai, Y.; Wu, H.-C.; Tran, H.; Mun, J.; Zheng, Y.-Q.; Tok, J. B.-H.; Gu, X.; Bao, Z. Tuning the Mechanical Properties of a Polymer Semiconductor by Modulating Hydrogen Bonding Interactions. *Chem. Mater.* **2020**, *32* (13), 5700–5714. https://doi.org/10.1021/acs.chemmater.0c01437.
- (59) Laysandra, L.; Njotoprajitno, A.; Prakoso, S. P.; Chiu, Y.-C. From Stretchable and Healable to Self-Healing Semiconducting Polymers: Design and Their TFT Devices. *Mater. Adv.* **2022**, 3, 7154-7184. https://doi.org/10.1039/D2MA00581F.
- (60) Rahmanudin, A.; Yao, L.; Sivula, K. Conjugation Break Spacers and Flexible Linkers as Tools to Engineer the Properties of Semiconducting Polymers. *Polym J* **2018**, *50*(8), 725–736. https://doi.org/10.1038/s41428-018-0069-z.
- (61) Melenbrink, E. L.; Hilby, K. M.; Choudhary, K.; Samal, S.; Kazerouni, N.; McConn, J. L.; Lipomi, D. J.; Thompson, B. C. Influence of Acceptor Side-Chain Length and

- Conjugation-Break Spacer Content on the Mechanical and Electronic Properties of Semi-Random Polymers. *ACS Appl. Polym. Mater.* **2019**, *1* (5), 1107–1117. https://doi.org/10.1021/acsapm.9b00115.
- (62) Kazerouni, N.; Melenbrink, E. L.; Das, P.; Thompson, B. C. Ternary Blend Organic Solar Cells Incorporating Ductile Conjugated Polymers with Conjugation Break Spacers. *ACS Appl. Polym. Mater.* **2021**, *3* (6), 3028–3037. https://doi.org/10.1021/acsapm.1c00213.
- (63) Lin, Y.-C.; Matsuda, M.; Chen, C.-K.; Yang, W.-C.; Chueh, C.-C.; Higashihara, T.; Chen, W.-C. Investigation of the Mobility–Stretchability Properties of Naphthalenediimide–Based Conjugated Random Terpolymers with a Functionalized Conjugation Break Spacer. *Macromolecules* 2021, 54 (16), 7388–7399. https://doi.org/10.1021/acs.macromol.1c00534.
- (64) Zhao, Y.; Zhao, X.; Zang, Y.; Di, C.; Diao, Y.; Mei, J. Conjugation-Break Spacers in Semiconducting Polymers: Impact on Polymer Processability and Charge Transport Properties. *Macromolecules* **2015**, *48* (7), 2048–2053. https://doi.org/10.1021/acs.macromol.5b00194.
- (65) Savagatrup, S.; Zhao, X.; Chan, E.; Mei, J.; Lipomi, D. J. Effect of Broken Conjugation on the Stretchability of Semiconducting Polymers. *Macromolecular Rapid Communications* **2016**, *37*(19), 1623–1628. https://doi.org/10.1002/marc.201600377.
- (66) Gasperini, A.; Bivaud, S.; Sivula, K. Controlling Conjugated Polymer Morphology and Charge Carrier Transport with a Flexible-Linker Approach. *Chem. Sci.* **2014**, *5* (12), 4922–4927. https://doi.org/10.1039/C4SC02073A.
- (67) Reeves, B. D.; Grenier, C. R. G.; Argun, A. A.; Cirpan, A.; McCarley, T. D.; Reynolds, J. R. Spray Coatable Electrochromic Dioxythiophene Polymers with High Coloration Efficiencies. *Macromolecules* **2004**, *37* (20), 7559–7569. https://doi.org/10.1021/ma049222y.
- (68) Zayat, B.; Das, P.; Thompson, B. C.; Narayan, S. R. *In Situ* Measurement of Ionic and Electronic Conductivities of Conductive Polymers as a Function of Electrochemical Doping in Battery Electrolytes. *J. Phys. Chem. C* **2021**, *125* (14), 7533–7541. https://doi.org/10.1021/acs.jpcc.0c08934.
- (69) Magdău, I. B.; Miller, T. F. Machine Learning Solvation Environments in Conductive Polymers: Application to ProDOT-2Hex with Solvent Swelling. *Macromolecules* **2021**, 54, 3377–3387. https://doi.org/10.1021/acs.macromol.0c02132.
- (70) Thurn-Albrecht, T.; Thomann, R.; Heinzel, T.; Hugger, S. Semicrystalline Morphology in Thin Films of Poly(3-Hexylthiophene). *Colloid & Polymer Science* **2004**, *282* (8), 932–938. https://doi.org/10.1007/s00396-004-1100-9.
- (71) Tashiro, K.; Ono, K.; Minagawa, Y.; Kobayashi, M.; Kawai, T.; Yoshino, K. Structure and Thermochromic Solid-State Phase Transition of Poly (3-Alkylthiophene). *J. Polym. Sci. B Polym. Phys.* **1991**, *29* (10), 1223–1233. https://doi.org/10.1002/polb.1991.090291007.
- (72) Jiao, X.; Statz, M.; Lai, L.; Schott, S.; Jellett, C.; McCulloch, I., et al., Resolving Different Physical Origins toward Crystallite Imperfection in Semiconducting Polymers:

- Crystallite Size vs Paracrystallinity. *J. Phys. Chem. B* **2020**, 124, 46, 10529–10538. https://doi.org/10.1021/acs.jpcb.0c06763.
- (73) Yavuz, I.; Martin, B. N.; Park, J.; Houk, K. N. Theoretical Study of the Molecular Ordering, Paracrystallinity, And Charge Mobilities of Oligomers in Different Crystalline Phases. *J. Am. Chem. Soc.* **2015**, 137, 8, 2856–2866. https://doi.org/10.1021/ja5076376.
- (74) Kline, R. J.; McGehee, M. D.; Kadnikova, E. N.; Liu, J.; Fréchet, J. M. J.; Toney, M. F. Dependence of Regioregular Poly(3-hexylthiophene) Film Morphology and Field-Effect Mobility on Molecular Weight. *Macromolecules* **2005**, 38, 8, 3312–3319 https://doi.org/10.1021/ma047415f.
- (75) Dong, B. X.; Smith, M.; Strzalka, J.; Li, H.; McNeil, A. J.; Stein, G. E.; Green, P. F. Molecular Weight Dependent Structure and Charge Transport in MAPLE-deposited Poly(3-hexylthiophene) Thin Films. *J. Polym. Sci. Part B: Polym. Phys.* **2018**, *56*(8), 652–663. https://doi.org/10.1002/polb.24588.
- (76) Kim, J.-H.; Nizami, A.; Hwangbo, Y.; Jang, B.; Lee, H.-J.; Woo, C.-S.; Hyun, S.; Kim, T.-S. Tensile Testing of Ultra-Thin Films on Water Surface. *Nat Commun* **2013**, *4*(1), 2520. https://doi.org/10.1038/ncomms3520.
- (77) Wang, Y.; Zhang, S.; Freychet, G.; Li, Z.; Chen, K.-L.; Liu, C.-T.; Cao, Z.; Chiu, Y.-C.; Xia, W.; Gu, X. Highly Deformable Rigid Glassy Conjugated Polymeric Thin Films. *Adv. Funct. Mater.* **2023**, 2306576. https://doi.org/10.1002/adfm.202306576.
- (78) Savagatrup, S.; Printz, A. D.; O'Connor, T. F.; Zaretski, A. V.; Rodriquez, D.; Sawyer, E. J.; Rajan, K. M.; Acosta, R. I.; Root, S. E.; Lipomi, D. J. Mechanical Degradation and Stability of Organic Solar Cells: Molecular and Microstructural Determinants. *Energy Environ. Sci.* **2015**, *8*(1), 55–80. https://doi.org/10.1039/C4EE02657H.
- (79) O'Connor, B.; Chan, E. P.; Chan, C.; Conrad, B. R.; Richter, L. J.; Kline, R. J.; Heeney, M.; McCulloch, I.; Soles, C. L.; DeLongchamp, D. M. Correlations between Mechanical and Electrical Properties of Polythiophenes. *ACS Nano* **2010**, *4* (12), 7538–7544. https://doi.org/10.1021/nn1018768.
- (80) Choi, J.; Kim, W.; Kim, D.; Kim, S.; Chae, J.; Choi, S. Q.; Kim, F. S.; Kim, T.-S.; Kim, B. J. Importance of Critical Molecular Weight of Semicrystalline n-Type Polymers for Mechanically Robust, Efficient Electroactive Thin Films. *Chem. Mater.* 2019, 31, 9, 3163–3173. https://doi.org/10.1021/acs.chemmater.8b05114.
- (81) Zheng, Y.; Yu, Z.; Zhang, S.; Kong, X.; Michaels, W.; Wang, W.; Chen, G.; Liu, D.; Lai, J.-C.; Prine, N.; Zhang, W.; Nikzad, S.; Cooper, C. B.; Zhong, D.; Mun, J.; Zhang, Z.; Kang, J.; Tok, J. B.-H.; McCulloch, I.; Qin, J.; Gu, X.; Bao, Z. A Molecular Design Approach towards Elastic and Multifunctional Polymer Electronics. *Nat Commun* **2021**, *12* (1), 5701. https://doi.org/10.1038/s41467-021-25719-9.